Meitner-Auger Electron Emitters for Targeted Radionuclide Therapy: Mercury-197m/g and Antimony-119

Parmissa Randhawa[1], **Aeli P. Olson**[2], **Shaohuang Chen**[1,3], **Kaley Lexi Gower-Fry**[1], **Cornelia Hoehr**[3,*], **Jonathan W. Engle**[2,*], **Caterina F. Ramogida**[1,3,*], **Valery Radchenko**[3,4,*]

[1]Chemistry, Simon Fraser University, Burnaby, BC, Canada

[2]Medical Physics and Radiology, University of Wisconsin, Madison, WI, USA

[3]Life Sciences, TRIUMF, Vancouver, BC, Canada

[4]Chemistry, Science, University of British Columbia, BC, Canada

Abstract

Targeted Radionuclide Therapies (TRTs) based on Auger emitting radionuclides have the potential to deliver extremely selective therapeutic payloads on the cellular level. However, to fully exploit this potential, suitable radionuclides need to be applied in combination with appropriate delivery systems. In this review, we summarize the state-of-the-art production, purification, chelation and applications of two promising candidates for Targeted Auger Therapy, namely antimony-119 (^{119}Sb) and mercury-197 (^{197}Hg). Both radionuclides have great potential to become efficient tools for TRT. We also highlight our current progress on the production of both radionuclides at TRIUMF and the University of Wisconsin.

Keywords

Targeted Radionuclide Therapy (TRT); auger electrons; mercury-197 (^{197}Hg); antimony-119 (^{119}Sb); production, radiochemical separation; coordination; imaging; dosimetry

1. INTRODUCTION

1.1. Nuclear Medicine

Radiopharmaceuticals exploit the intrinsic properties of radionuclides, harnessing their radioactive emissions for medical applications. Direct injection of a radiopharmaceutical into the bloodstream and subsequent localized accumulation in the region of interest has proven to be a targeted, non-invasive method to image and treat cancerous and diseased

*Address correspondence to this author at Life Sciences Division, TRIUMF, 4004 Wesbrook Mall, Vancouver BC, Canada; V6T 2A3; Tel/Fax: +1-604-222-7527, +1-604-222-1074: vradchenko@triumf.ca.

d(0.95)

e33.40 (1.03)

cells [1]. The injected radionuclide is often conjugated to a biological targeting vector *via* a chelating ligand to accomplish delivery of the radiometal payloads that would not normally form covalent bonds with pharmacological targeting vectors with avidity for the tumour tissue (typically through biomolecule/receptor interactions) [2]. Diagnostic radionuclides include positron (β^+) and gamma-ray (γ) emitters for positron emission tomography (PET) imaging or single-photon emission computed tomography (SPECT), respectively [3]. Emitted cytotoxic alphas (α), beta particles (β^-), and Meitner-Auger electrons can each be employed in targeted radionuclide therapy (TRT) [2].

Some radionuclides or selected radionuclide pairs (of the same or different elements) have both diag*nostic* and *thera*peutic emissions; a property colloquially referred to as "theranostic." Alpha or beta-emitting theranostic radionuclides have recently generated a significant interest (see. *e.g.*,[4-11]). This review focuses on two Meitner-Auger electron-emitting radionuclides as radiolabels in TRT, mercury-197 ($^{197m/g}$Hg) and antimony-119 (^{119}Sb).

1.2.   Meitner-Auger Electrons

The Auger effect and Auger electron discovery were believed to be contributed to science by Pierre Auger, a French physicist, in 1923 [12]. Historians have found that the effect was also observed and reported in the literature by the Austrian-Swedish nuclear physicist, Lise Meitner in 1922 [13, 14]. The Noble Prize for this discovery was awarded to Auger, although Meitner had an equal part in the discovery. Consequently, this paper will refer to the Auger electron as the Meitner-Auger electron (MAE).

MAE's are atomic electrons emitted during electron capture (EC) and/or internal conversion (IC) decay processes [15]. Multiple MAEs (5 to 50) can be emitted per decay as a result of an electron cascade, which occurs until all inner electron shell vacancies are filled. In addition to MAEs, EC and IC decay can produce conversion electrons (CE), X-ray emissions and Coster-Kronig (CK) and super-Coster-Kronig (sCK) transitions, all of which have therapeutic effects. The probability of DNA damage depends on electron energy [16]; the general energy trend follows CE>MAE>CK~sCK [16-18].

MAEs are low energy electrons (1-10 keV) with short path lengths (l-20μm, less than one cell diameter), resulting in a high linear energy transfer (LET, 4-26 keV/μm) (Fig. 1) [2], and thus a highly selective therapeutic radiation dose at the cellular level. However, the radioactive nuclide needs to be internalized within the cell or nucleus to have a maximum effect [19]. Studies have shown that when the MAE emitter is placed inside the nucleus, the MAEs induce a dose to the nucleus and DNA 30-times higher compared to if the radionuclide were located on the cellular membrane [16, 20-22]. However, therapeutic effects are still seen without nuclear internalization [23], suggesting that the relationship between radionuclide localization and cytotoxicity is incompletely understood.

Almost half of all medical radionuclides are MAE emitters. The most common radionuclides under investigation for MAE therapy are ^{125}I, ^{111}In, ^{67}Ga, ^{99m}Tc and ^{123}I, with ^{125}I being the most extensively studied (Table 1) [16]. However, most of these radionuclides are not necessary practically suitable for Auger Therapy, due to other accompanying

emissions (*e.g.*, photons for ^{111}In) or have half-lives incompatible for radiopharmaceutical use (*e.g.*, ^{125}I). The less explored nuclides antimony-119 ([119]Sb) and mercury-197m/g ([197m/g]Hg) show promising characteristics of an excellent MAE therapeutic agent due to their high MAE yields, high MAE energies, and reasonable half-lives [16, 17]. Though these radioisotopes have yet to make it into a wide-spread application, this review serves as a resource for radiopharmaceutical scientists to gain insight into how one might exploit these promising nuclides in their radiopharmaceutical research. Throughout this paper, we will discuss the applications and potential of these radionuclides as therapeutic and diagnostic agents, the production, purification, and chelation of [119]Sb and [197m/g]Hg.

2.　DOSIMETRY AND IMAGING OF [197m/g]Hg AND [119]Sb

As stated in Section 1.2, the therapeutic effectiveness of an MAE-based radiopharmaceutical is heavily dependent on its subcellular distribution and localization, along with other factors such as high MAE yields, high MAE energies, and half-lives. CE and MAE emissions have therapeutic potential as they possess cytotoxic amounts of ionizing radiation, which can cause irreversible damage to nuclear DNA (through double-strand or single-strand breakage), subsequently resulting in programmed cell death by apoptosis [15, 24-26]. MAE emitters are proven to give the highest cytotoxic effect when incorporated into the cellular DNA *via* nucleosides (*i.e.*, deoxyuridine and deoxycytidine) [27-30]. Increasing distance between the cellular DNA and the emitter decreases the cytotoxicity [30-32] due to their short pathlength, whilst the CEs contain a longer path length (0.05-12.00 mm) and do not require internalization into the cell to yield a therapeutic effect [25]. MAEs not located within the nucleus can cause damage *via* a secondary ionization mechanism by delivering oxidative stress to DNA (or other parts of the cell) through oxygen species (ROS), allowing for indirect damage outside the range of the emitter [16, 33]. The practical application of these MAE emitters requires the knowledge of potential dose amounts. A study by Humm *et al.* states to accurately calculate MAE dose, the half-life, emitted radiation, and interaction properties with the matter of the radionuclide are all critical, along with the radiochemical uptake and clearance data [17].

2.1.　Dosimetry of Mercury-197m/g

2.1.1.　The Decay Emissions of[197m/g]Hg—The decay emissions of [197m/g]Hg are useful for applications in both therapeutics (MAEs) and diagnostics (gamma rays), giving rise to a "theranostic" radionuclide. A theranostic pair of the same chemical element is favoured as biodistribution is expected to be equivalent in diagnostic and therapeutic applications, giving [197m/g]Hg a benefit over other theranostic pairs. However, attention needs must be paid to the decay of metastable to ground state mercury-197, which requires careful planning for the application of both forms for imaging and therapy, respectively. Moreover, this enables more individualized treatments, catered to a specific patient, through the ability to visualize the expected biodistribution of the treatment dose through imaging of tracer quantities of the radiopharmaceutical [18].

The available literature on the decay processes of [197m]Hg and [197g]Hg provides data on the gamma rays, branching ratios and MAE and CE emissions [34]. Studies recently published

in 2020 by Lebeda *et al.* have shown discrepancies in the gamma emissions and branching ratios in comparison to past studies [35, 36]. To address this, the discussion will reference the branching ratio and gamma-ray emissions determined by Lebeda *et al.* [35, 36], while the MAE and CE values discussed are produced by Walther *et al.* [34].

The two different energy states of mercury-197 (^{197m}Hg and ^{197g}Hg) differ by 299 keV; the two states lead to two distinct decay paths (Fig. 2) [18]. While ^{197g}Hg decays to stable ^{197}Au, ^{197m}Hg decays to either ^{197g}Hg by the isomeric transition (IT) or ^{197}Au* by electron capture with branching ratios of 94.68% and 5.32%, respectively [35, 36].

The more predominant decay, from ^{197m}Hg to ^{197}Hg, occurs by IT and results in a high energy gamma emission ([E_γ 164.84 keV, $I_\gamma = 0.2816\%$] and [E_γ 133.79 keV, $I_\gamma = 34.8\%$]), and a monoenergetic conversion electron (CE) (150 keV, 50%), as well as low energy MAEs with an average energy of 7.1 keV and L and K_α X-rays with average energies of 10 and 70 keV, respectively [18, 34-38].

Additionally, the ground state ^{197}Hg decays to an excited state ^{197}Au* through EC (523 keV, 100%). Further decay of the excited state ^{197}Au* to ground state ^{197}Au through IT results in a lower energy gamma-ray emission ([E_γ 77.31 keV, $I_\gamma = 0.0143\%$],[E_γ 268.78 keV, $I_\gamma = 0.0393\%$] and [E_γ 191.4371 keV, $I_\gamma = 0.632\%$]), a CE (63 keV, 60%), low energy MAEs with an average energy of 7.4 keV and L and K_α X-rays with average energies of 10 and 68 keV, respectively [18, 34-38].

^{197m}Hg can also decay directly to excited state ^{197}Au* through electron capture (EC) (499 keV, 5.32%). Further decay to ground state ^{197}Au by IT results in the emission of a high energy gamma-ray ([E_γ 130.00 keV, $I_\gamma = 0.1713\%$]. [E_γ 408.7 keV, $I_\gamma = 0.0057\%$]. [E_γ 278.65 keV, $I_\gamma = 3.79\%$] and [E_γ 201.39 keV, $I_\gamma = 0.0540\%$]) and a CE (116 keV, 6%) as well as low energy MAEs with an average energy of 7.6 keV and predominantly L and K_α X-rays with average energies of 10 and 70 keV, respectively [18, 34-38].

2.1.2. $^{197m/g}$Hg as a Therapeutic Radionuclide—The decay of ^{197m}Hg and ^{197g}Hg emits 19.4 and 23.2 MAEs per decay with average energies of 13.5 keV and 16.1 keV, respectively. The ground state (^{197g}Hg) is more suitable for MAE therapy as both the energy and number of MAEs emitted are greater than that of the metastable state and importantly ground state does not have a significant gamma emission component, which will affect the dosimetry. The average CE emitted per decay for ^{197m}Hg and ^{197g}Hg is 1.6 and 0.8, attaining energies of 203.5 keV and 54.1 keV, respectively [39].

Equivalent dose model calculations of ^{197m}Hg and ^{197g}Hg MAEs have been determined in the units mean absorbed doses per unit cumulated activity (Gray (Gy) per Becquerel (Bq)) for the ovaries, testes and liver for other emissions produce by $^{197m/g}$Hg and for the MAEs, utilizing a weighting factor of 20. These values can be seen in Table 2 [20]. This method of calculation takes into account the subcellular distribution of the radionuclides based on the organ, resulting in the mean equivalent dose increase when the organ activity localizes close to the DNA [20].

Mean absorbed dose values serve as a benchmark to predict the biological response for potential dose calculations of $^{197m/g}$Hg-radiopharmaceuticals. Although, when calculating dose amounts, the bystander effect must also be taken into consideration. Bystander effects result in the inhibition or enhancement of tumour cell growth in non-radio targeted cells, induced by a signal from labeled cells. The assessment of the bystander effect is essential to calculate an accurate dose as the actual radiobiological response will be greater/less than that predicted by dosimetric estimates alone [19].

The dose amounts of $^{197m/g}$Hg for therapy have not yet been determined to our knowledge as there have been no reported treatments utilizing $^{197m/g}$Hg; although, comparisons can be made with the FDA approved ^{111}In MAE emitter, which has a 2-fold lower MAE energy and 8-fold lower CE energy than $^{197m/g}$Hg [39]. ^{111}In labeled modular nanotransporter, radiopharmaceutical has been reported to successfully treat EJ xenograft tumours in mice when dose amounts of 9.2 MBq, 4.6 and 2.3 MBq were administered. The 4.6 and 2.3 MBq doses led to a decrease in the initial tumor size whereas, 9.2 MBq dose led to non-detectable amounts of initial tumor at the end of treatment (33 days) [40].

Based on potential therapeutic doses, only trace amounts (ng - µg) of $^{197m/g}$Hg will be required to induce a radiotherapeutic effect. This administered amount is far below the safe concentration limit of mercury in the blood set by Health Canada (0.1 µg/g for the average human; 4.5-9 mg)[a] [41, 42], the U.S. and Netherlands (0.7 µg/kg body weight), Japan (2.0 µg/kg), and Europe (1.6 µg/kg) [42-45]. Further, studies suggest clinical aid is needed for mercury blood concentration levels exceeding 25 µg/kg[b] (1,125-2,250 mg)[c] [46, 47] – several orders of magnitude above the amount needed for a therapeutic effect from $^{197m/g}$Hg radiopharmaceuticals, implying there is no risk of mercury poisoning by this treatment method.

2.1.3. $^{197m/g}$Hg as a Diagnostic Radionuclide—Recent studies utilizing a Philips BrightView SPECT camera yielded measurements that were verified by Monte Carlo simulations to prove the capabilities of ^{197m}Hg as a SPECT imaging radionuclide (Fig. 3) [18]. The emission photons with energies of 134 keV and 77 keV lie in the appropriate range (100-250 keV) for the SPECT low-energy high-resolution (LEHR) collimations and provide sufficient images with a resolution of 6 mm [18, 48, 49]. The imaging properties of $^{197m/g}$Hg offer diagnostic applications as well as aids in the determination of an appropriate therapeutic dose of the radiopharmaceutical by its biodistribution properties *in vivo.*

2.1.4. $^{197m/g}$ Hg vs 177 Lu FDA approved theranostic radionuclide—The diagnostic and therapeutic properties of $^{197m/g}$Hg have previously been compared to the commercial theranostic radionuclide Lutetium-^{177} (177Lu) [34]. $^{197m/g}$Hg produces 8 times more photons with energies of >50 keV than 177Lu, resulting in a gamma dose 6 times higher than ^{177}Lu [50]. The therapeutic dose per decay is 10 times higher for $^{197m/g}$Hg in a small radius of 1 µm, as a result of the large number of MAEs emitted

---

[a]Calculated by utilizing the average mass of a human to be 45-90 kg.
[b]The mercury blood concentration levels in µg/kg were calculated from 25 µg/L assuming the density of blood is 1002 g/l.[222]
[c]Calculated by utilizing the average mass of a human to be 45-90 kg.

by $^{197m/g}$Hg. This further indicates the potential of $^{197m/g}$Hg as a theranostic agent, as its decay delivers appropriate emissions for nuclear medicine *in vivo* treatment and imaging of micrometastases and small tumors.

2.2. Dosimetry of Antimony-119

2.2.1. The Decay Emissions of^{119}Sb—A MAE emitting radionuclide with highest energy photon emission of 29.1 keV, ^{119}Sb ($t_{1/2}$ = 38.19 h, EC = 100%) provides high LET deposition and clean dose profiles (Fig. 4) [51, 52]. Decaying by electron capture, ^{119}Sb emits an average of 24 internal conversion and MAEs per decay [53].

2.2.2. ^{119}Sb as a Therapeutic Radionuclide—A mathematical model evaluating the relationship between tumor-to-normal-tissue mean absorbed dose-rate ratio (TND) and electron energy was created by [54] to survey low energy electron emitters suitable for small tumor radionuclide therapy. Based on this model, they determined that a radionuclide ideal for small tumor radionuclide therapy as seen by high TND would have the following qualities: (1) emitted electron energy less than 40 keV, (2) a photon--to-electron ratio below 2, (3) half-life between 30 min and 10 days, (4) stable daughter nuclide or half-life no longer than 60 days, (5) production *via* neutron capture or proton-, deuteron-, alpha particle-induced reaction, and (6) exclusion of Nobel gases due to unsuitable labelling chemistries. From this criteria, five nuclides, including ^{119}Sb (^{103m}Rh, ^{161}Ho, ^{58m}Co, and ^{189m}Os) were determined suitable for small tumor radiotherapy application, contingent on the development of selective targeting vectors for cellular internalization [54]. The additional analysis estimated 100 GBq ^{119}Sb activity would be required for 2 Gy whole-body dose, requiring high molar activities to avoid target saturation [54].

Having yet to be introduced into living systems, dosimetric calculations have been used to assess the targeted radiotherapeutic capacity of ^{119}Sb. In 2008 [55], calculated MIRD S-values and theoretical dose distributions for ^{119}Sb in various intercellular locations. Dose distributions from various radionuclides in a spherical 8 μm radius cell with 6 μm nuclear radius were compared against one another, and ^{119}Sb delivered the highest dose to the nucleus (Fig. 5) of compared nuclides when activity was uniformly distributed along the cell surface [55].

Using the Monte Carlo PENELOPE code and a Monte Carlo damage simulation code [56], calculated cellular S-values for ^{119}Sb and compared them against other promising MAE emitting radionuclides to calculate biological effectiveness. More than 75% of single and double-strand breaks occurred in regions within 2.5 μm of the center of the nucleus, with ^{119}Sb providing the second-highest number of single and double-strand DNA breaks of the nuclides tested (see Table 3) [56].

In living systems, cellular geometry is irregular, so the study [57] explored the impact of off-centered nuclei on subsequent cellular S-value calculations for 12 relevant radionuclides. For ^{119}Sb, eccentricity had an extremely large effect on subsequent S-value calculation as seen by an increase in S-value (N←CS) of the off-centered nucleus is closer to the cell surface and lower energy electrons can reach the nucleus and add dose [57]. Reasonably, the study [57] also shows a decrease in cellular S-value (N←Cy) as the nucleus becomes

more off-centered as cytoplasm is displaced and activity subsequently further from the nucleus. For radionuclides such as [119]Sb, it is imperative to use Monte Carlo code with event-by-event simulation in order to have an adequate spatial resolution or else suffer an underestimation of secondary electrons, which greatly underestimates energy deposition [57]. Table 4 compares [119]Sb nucleus-to-nucleus S--value as reported within the literature for various cell and nuclear radius.

2.2.3. [119]Sb as a diagnostic agent

Having few low energy x-ray and gamma emissions (E_γ 23.9 keV, I_γ = 16.0%) [53], [119]Sb is well suited for therapeutic application as seen by photon/electron ratio 0.9 [55]. Antimony-117 (2.8 h, E_γ 158.6 keV, I_γ = 85.9%) has been proposed as a radioisotopic imaging analogue, and shown [55] to provide adequate imaging capabilities. Using a Jazczak phantom depicted in Fig. 6, planar scintigraphy (left) and SPECT images (right) distinguishing all cold rods in the scintigraphy image, the three largest cold spheres (ø38 mm, ø31.8 mm, and ø25.4 mm) in SPECT image, and a modelled hot tumor over background signal [55].

3. PRODUCTION OF [197m/g]Hg AND [119]Sb

3.1. Production of [197m/g]Hg

Mercury-197,[197]Hg ($t_{1/2}$ 64.14 h, E_{Auger} 7.4 keV) [58], is a well-known gamma-ray radiation standard [59]. The metastable state of this isotope, [197m]Hg, has a shorter half-life of 23.8 hours and its decay results in the emission of 134 keV gamma-rays [58]. [197]Hg has been applied to brain scans as early as the late 1960s [60], but medical use ceased not long after due to the high toxicity and long biological half-life of mercury compounds *in vivo* (*vide infra*). One key requirement for the implementation of [197m/g]Hg radiopharmaceuticals is the availability of radioisotope with high radionuclidic and chemical purity. Below we discuss the *via*ble production methods for [197m/g]Hg.

3.1.1. Production of[197m/g]Hg via Cyclotron

The production of [197m/g]Hg *via* cyclotron can be achieved by proton or deuteron irradiation of natural gold. In nature, gold is comprised of only one stable isotope, [197]Au, which is a great advantage for producing [197m/g]Hg as the target does not need to be isotopically enriched. The maximum total cross-section for the [197]Au(p,n)[197m/g]Hg reaction is 93 mb at 11.3 MeV [61]. Cyclotron production of [197]Hg has a few advantages over other methods. The most prominent asset is the high specific activity achievable of the product nuclide [34]. Secondly, with sufficient production cross-section with low to medium energy protons, mercury $^{-197}$ can be made available in many research centres. For production with protons, the ratio at the end of bombardment for metastable and ground states of mercury^{-197} is 50/50.

3.1.2. Production of [197m/g]Hg via Neutron Generator and other Methods—

There are other production routes for this radioisotope. For example, irradiation of enriched [196]Hg with thermal neutrons can also be used to generate [197]Hg *via* neutron capture [62]. However, this production route requires enriched mercury material, making it less cost-effective, and during the irradiation, long-lived [203]Hg contaminants according to the enrichment level [34]. Additionally, [197]Hg may be formed by another costly method with

limited access – fragmentation of heavier elements such as lead (Pb) with energetic protons (>100 MeV) [63].

3.1.3.   Production of [197m/g]Hg at TRIUMF—At TRIUMF, [197m/g]Hg is produced on the TR13 (13 MeV) cyclotron *via* the [197]Au(p,n)[197m/g]Hg reaction on solid gold targets. The targets are manufactured by sintering on tantalum backings of 28 mm diameter. Tantalum is chosen for its high melting point (> 3000°C), machinability, and relatively low cost. To make the target, 200–270 mg of metallic gold is placed in the 0.25 mm deep, 10 mm OD indent (see Fig. 7 and pressed under ~7 MPa, giving an 0.13 mm thickness assuming metal-bulk density. According to SRIM-2013 simulations, 0.265 mm of gold is needed to fully stop 13 MeV protons [64]. Then, the gold is sintered onto the tantalum in a furnace (Rd-G – RD Webb Company – Natick MA, USA) at 1150°C for about an hour and cooled for eight hours.

After preparation, the target is loaded into the TRIUMF TR13 cyclotron solid target station [65]. An aluminum foil separates the gold target from the cyclotron vacuum and allows helium cooling on the front face. The tantalum rear side is cooled with cooling water. The target is irradiated with 12.8 MeV protons at a beam current of 20 μA for up to four hours. Target removal is performed the next day after a cool-down period to lower the radiation exposure to cyclotron operators. Typically, the activity of the irradiated gold target is measured about one day after the end of the beam by a dose calibrator (Capintec®–55tR) with a built-in calibration for [197]Hg. We are currently working to employ gamma-spectroscopy for the accurate characterization of produced quantities of [197m]Hg and [197g]Hg. There is also potential to increase the production yield by extending irradiation time and current. Additionally, larger gold deposition on the target can be applied [58].

3.1.4.   Production of [197m/g]Hg at TRIUMF via Gold Nanoparticles—An alternative to the irradiation of a solid gold target is the irradiation of gold nanoparticles (AuNP) suspended in a liquid. The radiometal production in a solution target is especially attractive for sites without a solid target station, and has been applied to the production of radiometals like ^{68}Ga, [86]Y, [89]Zr, [94m]Tc or [44]Sc, see *e.g* [66-75]. In addition, the produced [197m/g]Hg is embedded in the AuNP and can then be used for radiotherapy applications directly.

As proof of principle at TRIUMF, a solution of 5×10^{19} np/ml (equivalent of 0.063 mg/ml of gold) of 5 nm AuNP immersed in deionized water was prepared. The solution was loaded into a liquid target [76] and irradiated with 12.0 MeV protons with a beam current of 20 μA for 30–40 min. The target was then flushed with deionized water into a 20 ml vial. Gamma spectroscopy validated the presence of [197]Hg in the solution, see Fig. 8. However, when a low AuNP concentration is used as in tins example, yields are only 10.2 ± 0.4 kBq and 10.4 ± 0.9 kBq for a 40 min irradiation for [197g]Hg and [197m]Hg decay corrected to end of bombardment, respectively.

3.2.   Production of [119]Sb

Production of [119]Sb for medical application has been explored through two main routes: directly *via* charged particle bombardment of tin or indirectly *via* the production of [119]Te

and subsequent development of ^{119}Te/^{119}Sb generator. Possible nuclear reactions, reaction Q values [77], and location of subsequent cross-section measurements are summarized in Table 5. Direct production of ^{119}Sb is a no carrier added method, innately providing higher apparent molar activity than indirect production as residual trace ^{nat}Sb target material will be loaded onto the generator system.

3.2.1.   Production of ^{119}Sb by Direct Production—The feasibility of each nuclear reaction for ^{119}Sb production depends upon many things, including reaction cross-sections, target design, co-produced radionuclidic impurities, and the availability of suitable accelerators. The broad availability of cyclotrons capable of accelerating protons 7-16 MeV, lack of radionuclidic impurities, and high relative yield favor the ^{119}Sn(p,n)^{119}Sb reaction, allowing no carrier added production. Direct production for medical application was first developed at the Hevesy Laboratory [55, 78, 79], who reported thin target (5.5 mg/cm^2) ^{119}Sb end of bombardment (EOB) yields from electroplated 97.4% enriched ^{119}Sn of 1.85 ± 0.12 MBq/µAH. Tin targets were made from 0.25 M KOH based electrolytic solutions at 65-70 °C and current density 4-6 mA/cm^2 for 6-8 h [55]. Slanted target geometries were employed to further increase yields, spreading beam current power over a larger water-cooled surface area. They report a maximum beam current target tolerance of 180 µA, thermal power density 1.02 kW/cm^2, a heroic feat considering the low melting temperature (231.93 °C) of tin, and extrapolate measured ^{nat}Sn bombardment yields to a hypothetical 46 GBq of ^{119}Sb from a 30 mg/cm^2 slant target with 97.4% ^{119}Sn enrichment, irradiated with 150 µA 16 MeV protons for 3 h [78].

Prior work in Sn target fabrication is built upon by [80] optimizing electroplating variables and developing an Sn sedimentation process. Resultant mean target thickness (39.3 µm) is reported for targets created by sedimentation, though thermal shock testing caused losses in target integrity prior to irradiation experiments. Again, potassium hydroxide alkaline-based electrolytic solutions out-perform acidic electrolytic solutions; the most favorable deposition conditions of 40 g/L Sn, 75 °C, and 50 mA/cm^2 current density resulted in targets with unreported thickness. To increase yields without increasing target thickness [80], also designed inclined targets (6°). The target withstood 160 µA beam current intensities for 10 min with no observed degradation, but ^{119}Sb yields were not reported. The anticipated radionuclidic impurities ^{122}Sb, ^{120m}Sb, ^{118m}Sb, and ^{117}Sb were observed with production yields of 2.19 MBq/µAh, 807 kBq/µAh, 46.1 MBq/µAh, and 430 MBq/µAh, respectively [80]. The group catalogs their process and many attempted trials as well as provide detailed quality control analysis, including homogeneity, morphology measured *via* scanning electron microscopy, and stability to thermal shock tests. Target fabrication methods were not applied to enriched material, perhaps because of the high cost of this material (6 USD/ mg).

3.2.2.   Production of ^{119}Sb by Indirect Production—Tellurium-119m/g (t$_{1/2}$ = 4.7 d/16.0 h) are the radioactive parents of Sb-119 (t$_{1/2}$ = 38.5 h) and therefore a potential feedstock in a transient equilibrium generator system allowing ^{119}Sb access to clinics without cyclotron production capabilities [81]. Production of ^{119}Te begins with proton irradiation of ^{nat}Sb *via* (p,3n) and (p,5n) reactions on the two naturally occurring stable

isotopes of antimony (^{121}Sb and ^{123}Sb) [82-86]. In 1992 [83], developed a precipitation method for separated ^{119}Te from ^{nat}Sb target material, involving two solution matrix changes to co-precipitate Te and final distillation. Purified Te solution was used for further generator development. They measured 82% retention of tellurium and estimated radionuclide purity at >99%; radioantimony activity was below detection limits [82].

A remotely handled radiochemical separation of ^{119}Te from medium energy proton irradiated ^{nat}Sb targets was developed at Los Alamos National Laboratory [84]. The fourstep separation process sequentially used CL resin (99% ^{119}Te efficiency), Rare Earth resin (97% ^{119}Te efficiency), AG 1-X8 anion (97% ^{119}Te efficiency), and a Pre-Filter Resin (100% ^{119}Te efficiency) to remove excess sulphur and phosphor) to separate 10^{16} atoms (100 nmol) of ^{119m}Te from grams (200 mmol) of ^{nat}Sb. Throughout chemical separation development, X-ray absorption near edge structure (XANES) and extended X-ray absorption fine structure (EXAFS) measurements characterized Te and Sb oxidation and speciation in various aqueous matrices and on solid-state chromatographic supports. This innovative analytical approach helped develop a system, which reduced antimony target mass from 25 g to approximately 28 mg (2 ppm ^{nat}Sb in 14 mL final volume), a separation factor of 10^3 [84].

In generator development studies, a combination ionexchange column comprised of 1 cm neutral grade alumina and 4 cm $SnO_2[H^+]$ was found to elute a maximum ^{118}Sb-tartrate yield of 12.5% at pH 3.5 with a corresponding 0.12% ^{118}Te breakthrough [87]. Activated carbon as an adsorbent for generator creation has been studied [82]. Activated carbon was pulverized and sorted with 120-180 mesh sieve, slurried with deionized water, and packed into a 2.5 mL plastic pipette tip between two plugs of fine glass wool. Previously separated radiotellurium HCl based solution was adjusted to various pHs using NaOH and passed through the tip. Distribution was tracked with ^{118}Te and ^{118}Sb tracers. Optimal Te(IV) loading occurred at pH=7-8 with no adsorption of Sb(V) in pH 4-10. 5 mL boluses of various mobile phases were tested for ^{118}Sb elution and ^{118}Te breakthrough over 9 days. Borate (0.2 M) mobile phases had the highest ^{118}Sb yields (35-48%) and lowest ^{118}Te breakthrough (0.3-1.7%) [82].

Activated carbon-based systems were also optimized as ^{118}Te/^{118}Sb generators. After anion-exchange based separation of radiotellurium from dissolved ^{nat}Sb, the target solution was diluted to 9M HCl and 18 mg/mL Sb. The column was washed with 2 M HCl and radiotellurium (^{118}Te, ^{119}Te, ^{121m}Te) was eluted in deionized water. This new anionexchange separation recovered 87-89% of the tellurium radioisotopes with no detectable antimony-118. Tellurium elution was adjusted to pH 8 using NaOH and loaded onto activated charcoal columns sifted to mesh size either 120-180 or 180-300. Various mobile phases and mild oxidizers were monitored for generator optimization, as Sb(V) and Sb(III) were shown to have different column affinities. Monitoring the oxidation state of eluted Sb provides information about the oxidation state distribution of Sb post-Te decay. Comparing the ratio of antimony eluted with and without the use of oxidizing agent provided oxidation state ratio of antimony post tellurium decay of 61% ^{118}Sb(III) and 39% ^{118}Sb(V). Maximum recovery of ^{118}Sb was 85-88% in 0.12M boric acid / 0.020 M borax / 3.5 mM NaOCl, with ^{118}Te breakthrough of 0.01-0.07% by activity [85].

Production *via* Te/Sb generator confronts difficulties on three fronts. Firstly, because Te is separated from natural antimony target, residual macroscopic stable Sb is difficult to fully separate and thus will be loaded onto the generator system. The presence of stable Sb poses a problem to chelation and will decrease the apparent molar activity of subsequent radiopharmaceuticals. Secondly, a generator needs to be developed with low tellurium breakthrough, lest tellurium contaminates eluent, and the solution gains a radioimpurity with dosimetric and chelation competition implications. Thirdly, being produced from proton bombardment of natural antimony, multiple radiotellurium isotopic impurities are produced, which decay to multiple radioantimony isotopic impurities, specifically ^{117}Sb and ^{118}Sb. Though (p,3n) reaction upon ^{121}Sb produces the desirable ^{119}Te, when using natural isotopic enrichment, ^{121}Te is also created, which decays to stable ^{121}Sb. This radiotellurium contamination would decrease molar activity by introducing more stable antimony into the system.

The aforementioned production routes have differing dosimetric implications. Tellurium-121 ($t_{1/2}$ = 119.2 d, E_γ 573 keV, I_γ = 80.4%) is a significant radioimpurity in the generator systems produced *via*^{nat}Sb irradiation that, though it decays to stable ^{121}Sb, provides a radiation safety challenge. Shielding generator operators from 573 keV photon emission would be required. The (p,pn) side reaction induced upon ^{nat}Sb produces ^{120}Sb ($t_{1/2}$=5.76 d, E_γ 1171.7 keV, I_γ = 100%) and ^{122}Sb ($t_{1/2}$=2.72 d, E_γ 564.2 keV, I_γ = 70.7%) [51]. These radionuclidic impurities loaded onto the generator will provide radioantimony impurities that increase radiation dose administered into the patient, especially considering a chelator would chelate the radioantimony and introduce it into the system. The (p,4n) and (p,5n) reactions upon ^{123}Sb produce ^{118}Te and ^{117}Te, respectively. These two radiotellurium impurities will feed ^{117}Sb ($t_{1/2}$ = 2.8 h, E_γ 158.6 keV, I_γ = 85.9%) and ^{118}Sb ($t_{1/2}$ = 5 h, E_γ 1229.6 keV, I_γ = 100%) into the system [51]. Though ^{117}Sb is an imaging analogue, these two radioantimony impurities have high yield emissions of high energy photons, delivering extra dose to patients and those handling/preparing radiopharmaceutical injections.

4. PURIFICATION OF $^{197m/g}$Hg AND ^{119}Sb

4.1. Radiochemical Separation of $^{197m/g}$Hg

4.1.1. Radiochemical Separation of $^{197m/g}$Hg via a Dowex 50 Resin—Macnevin and Lee separated 8 g of mercury from 400 g of gold [88]. In their experiments, gold and mercury were loaded into a large column containing 800 grams of Dowex 50 resin by 2 M hydrochloric acid. Gold was eluted with water, and mercury was eluted with 2 M HCl. In this study, it is also stated that a preliminary study with small amounts of gold and mercury was carried out, but their exact amount remains unclear.

4.1.2. Radiochemical Separation of$^{197m/g}$Hg via a Amberlite IR-120/400 Resin —In 1972, Gupta and Tandon also performed a series of studies aiming at the separation of mercury from several other metal ions [89]. Instead of Dowex 50, they experimented with the strong cation exchanger Amberlite IR-120 and a strong anion exchanger Amberlite IR-400. They revealed that mercury and gold can be loaded onto the strong anion exchanger at 0.6 M HCl. Gold can be selectively eluted from the resin by 0.6 M HCl – 90%

tetrahydrofuran, before the elution of mercury with nitric acid of high concentration. Meanwhile, they also determined that mercury shows a very little affinity towards Amberlite-120, even at low acid concentrations. This result seems to contradict the findings of Macnevin and Lee as in both cases, a strong cation exchanger was applied, although the exact type of strong cation exchanger in the two studies differs [88].

4.1.3. Radiochemical Separation of $^{197m/g}$Hg via a Chelex 100 Resin—Chelex 100 resin is a styrene-divinylbenzene copolymer containing paired iminodiacetate ions, which act as chelating groups in binding polyvalent metal ions. Meanwhile, the carboxylic acid groups of this resin classify it as a weak cation exchanger. Samczyński studied the ion exchange behaviour of a few elements covering mercury and gold and discovered that mercury taken up by Chelex 100 can be eluted with 10 M HCl, whereas gold is extremely strongly held in the whole range of HCl concentrations [90]. Removal of gold was attained by means of a solution of ammonia containing ammonium chloride. Unfortunately, the amounts of mercury and gold used were not stated.

4.1.4. Radiochemical Separation of $^{197m/g}$Hg via a Dithizone Resin—Chelating resins can also be applied to separate mercury from the gold. For example, dithizone is a sulphur-containing organic compound and forms complexes with many metals such as mercury. Grote and Kettrup reported a method synthesising a resin with dithizone as functional groups [91]. Shah and Devi adopted this synthesis method and studied the separation of several binary mixtures, which included gold-mercury with this chelating resin [92]. Mercury was eluted with a 1:1 mixture of 0.2 mol.L^{-1} HNO$_3$ and 2.0% ammonium nitrate. Then elution of gold was performed with a 1:1 mixture of 0.1 mol·L^{-1} HCl and 1.0% thiourea solution. The main drawback of this method is that gold and mercury were loaded onto the resin in a pH 5 acetate buffer solution. Cyclotron production of ^{197}Hg often requires gold targets, which hardly dissolve under mild conditions. In order to leverage this method, dissolved targets must be treated to the suitable condition, which adds up processing time, leading to higher losses of the product nuclide due to decay.

4.1.5. Radiochemical Separation of $^{197m/g}$Hg via a Hexylthioglycolate Resin —Another sulphur-containing chelating resin was synthesised by Moyers and Fritz [93]. In their study, a highly cross-linked, microporous resin containing the hexylthioglycolate functional group was yielded. Mercury and gold can be readily retained by the resin in 0.1 M HCl. Subsequently, mercury can be eluted with 6 M HCl while gold remains adsorbed. The latter is not eluted by hydrochloric acid but is eluted with 0.001 M thiourea in pH 3.0 HCl without difficulty.

4.1.6. Radiochemical Separation of $^{197m/g}$Hg via Liquid-liquid Extraction— Liquid-liquid extraction (LLE) is another separation technique that can be adopted for gold-mercury separation. With a wide range of selections of organic solvents, by carefully choosing extracting agents, the selective separation of mercury from gold can be reached. Singh and Tandon studied the separation of mercury as chloride from four other metal elements, including gold [94]. However, in this study, gold was only partially taken up by the organic phase in one step with minor mercury co-extraction. It was argued that

mercury was extracted in practically negligible amount, but with regard to the radiochemical separation of ^{197}Hg where the mass of mercury is at the level of nanograms or even less, this "negligible amount" would be unacceptable.

Nayak and Lahiri reported co-extraction of gold and mercury using methyl isobutyl ketone (MIBK) from HCl solutions [95]. Alternatively, they adopted the extraction system comprising 0.1% Aliquat 336 and 6 M HNO$_3$. As a result, 92% of gold along with 54% Tl were extracted into the organic phase, leaving a handful of radionuclides in the aqueous phase, including ^{197}Hg. In the absence of other radioisotopes, this method can be implemented for ^{197}Hg/Au separation. It's noteworthy that the Au/Hg separation factor of 613 applying this procedure can be far too insufficient for the separation of cyclotron produced ^{197}Hg.

In 2015, Walther *et al.* outlined the extraction of gold with four times of 500 μL MIBK while the main part of mercury radionuclide (60 – 80%) remains in the 2 M HCl [63]. They also pointed out that in order to investigate the possible reduction of gold contents in ^{197}Hg solution, one probe was extracted six times instead of four times with MIBK. However, this comes at the price of more than 50% of the product being lost.

4.1.7.   Radiochemical Separation of$^{197m/g}$Hg via a LN Resin—Walther *et al.* came up with a resin-based method, which uses solid extraction as separation principles [96]. The LN resin, which is composed of di(2-ethylhexyl)orthophosphoric acid impregnated onto inert support, was applied. A comparably narrow product $^{197(m)}$Hg peak versus the broad peak for the elution of the gold target material was obtained. It is also stated that there are several advantages in using LN resin as compared to the previous MIBK LLE method: 1) higher separation factor, 2) better handling and possible automation, which significantly improves radiation protection, 3) significantly lower product losses during the separation, and 4) convenient recycling of the gold target material is possible.

4.1.8.   Radiochemical Separation of$^{197m/g}$Hg via a LN Resin at TRIUMF—At TRIUMF, a separation scheme based on extraction chromatography with the use of LN resin has been practised. The irradiated target unloaded from the TR13 cyclotron after the cool-down period was placed in a dose calibrator (Capintec®–55tR) to measure the ^{197}Hg activity. Then it is dissolved in aqua regia with electric heating at 90°C. This solution is then transferred into a column packed with LN resin (TrisKem International SAS, Bruz, France) preconditioned with 6 M HCl. Gold is retained under these conditions while mercury is quickly eluted. With the help of the dose calibrator, the first volumes of eluate with tiny activities are collected in a 20 mL glass vial. Then another 20 mL glass vial is used to collect the majority of ^{197}Hg, indicated by its activity. This mercury fraction is then evaporated on a hot plate with the heating temperature initially set at 60°C which is eventually raised to 160°C. When the volume decreases to the level of near dryness, heating is removed and about 1 mL 0.1 M HCl is added. This step is repeated twice. After the evaporation, the remaining solution in the vial is transferred into a smaller container. The former vial is then washed with 1–2 drops of 0.01 M HCl and the washing solution combined into a 2 mL HPLC vial to ensure that the majority of ^{197}Hg is recovered. The activity of the recovered ^{197}Hg is measured using the same dose calibrator setup.

The yield of ^{197}Hg is impacted by a few factors. In order to facilitate the subsequent evaporation process, reduction of initial product volume is of the essence. For this purpose, eluate containing minor ^{197}Hg activities is disposed of as radioactive waste, inducing a loss of this radioisotope. Moreover, every time the ^{197}Hg solution is transferred from one vessel to another, loss occurs due to its adsorption to vessel walls.

During evaporation, the ^{197}Hg solution cannot be evaporated to dryness because of the volatility of mercury compounds in HCl (pH<2). In order to maximise the specific activity of the final product, the volume to be left in the 20 mL glass vial must be closely monitored. If the evaporation is overdone, not only a majority of ^{197}Hg activity is lost, but the working surface and even personnel nearby can also be heavily contaminated by radioactive mercury.

In the last step of the experiment, the dissolved ^{197}Hg is transferred from the 20 mL glass vial to a 2 mL HPLC vial. If the former vial is not washed, there might be a significant loss of mercury activity.

4.2. Radiochemical Separation of ^{119}Sb

4.2.1. Radiochemical Separation of ^{119}Sb via Solvent Extraction—Solvent extraction method for the separation of antimony and other elements, especially tin and tellurium, has been extensively studied. White and Rose employed several extracting solvents: methyl acetate, ethyl acetate, butyl acetate, acetoacetic ester, acetylacetone, ethyl acrylate, chloroform, and carbon tetrachloride [97]. They determined that ethyl acetate was the best of the extracting liquids for the citrate-oxalate complex. Optimal extraction was in 1 to 2 M HCl. Over 99% of antimony(V) could be recovered in three extractions. Rhodamine-B determination indicated that tellurium and tin were not extracted.

Hagebø *et al.* reported the separation of antimony from tellurium and the isolation of fission-product tin [98]. After dissolving the irradiated tellurium target, tin(II) in excess was used to precipitate tellurium from the cold solution. Antimony(V) was then extracted from 9 M HCl into isopropyl ether. As for tin-antimony separation, less than one percent of antimony(V) was extracted by ethyl ether from 7 M ammonium thiocyanate solution in 0.5 M HCl. According to Bock, tin(IV) will be extracted completely (more than 99 percent) under these conditions [99].

4.2.2. Radiochemical Separation of ^{119}Sb via metal Complexation Followed by Solvent Extraction—A sequential separation of arsenic, antimony, bismuth and tin using a crown ether was introduced by Vibhute and Khopkar [100]. Bismuth was first extracted by 0.05 M 18-crown-6 in methylene chloride from 0.1 M sulphuric acid containing 0.075 M potassium iodide. Secondly, tin was removed from the aqueous phase with 0.04 M 18-crown-6 in methylene chloride from 0.75 M sulphuric acid containing 0.15 M potassium iodide. Finally, the aqueous phase, adjusted to 1 M sulphuric acid and 0.25 M potassium iodide concentration, was equilibrated with 0.02 M 18-crown-6 in methylene chloride to extract antimony. Arsenic remained in the aqueous phase in the entire procedure.

Solvent extraction separation of antimony(III) and bismuth(III) with Cyanex 302 was investigated by Sarkar and Dhadke [101]. Although the main focus of this study is the

separation of antimony and bismuth, ternary systems including Sb-Sn-Cd and Sb-Sn-Tl are also covered. For both ternary mixtures, antimony(III) was extracted by 1.0×10^{-2} M Cyanex 302 in toluene from 0.25 M H_2SO_4, while tin(IV) remains unextracted in the aqueous phase.

4.2.3.   Radiochemical Separation of [119]Sb via Precipitation—Precipitation methods may also be considered to separate antimony from tellurium or tin. Abecasis presented a fast separation method for antimony from tellurium, in which the total separation time was about 15 minutes [102]. After dissolving the target, the solution was conditioned to 3 M HCl. Tellurium was precipitated by hydrazine hydrochloride with heat and filtered. Antimony in the filtrate was precipitated by H_2S with heat being applied.

Precipitation can also be combined with other chemical processes to achieve a higher degree of purification. Menon *et al.* separated tin and antimony by an initial phosphate precipitation step, using the difference in the precipitation behaviour of tin and antimony phosphates [103]. The irradiated target was dissolved in 3 M HCl with the addition of Br_2-H_2O to oxidise tin and antimony to their corresponding highest oxidation state. Tin was precipitated as Sn(IV) phosphate from the hot solution by adding $(NH_4)_2HPO_4$ at pH ~1, while antimony was not precipitated as phosphate. Antimony was precipitated as sulphide form in later steps and this precipitate was further purified by the stibine method. However, in both studies presented above, carriers of antimony, tin and tellurium were used. As mentioned above, no carrier added radioisotopes are strongly desired in radiopharmaceuticals because they present high specific activity. For this reason, precipitation methods with added carriers may not be preferred for this intrinsic drawback.

4.2.4.   Radiochemical Separation of [119]Sb via a Dowex 50 Resin—Ion-exchange processes are commonly used to separate and purify metals. The study conducted by Kraus *et al.* found that in 12 M HCl, Sb(V) was adsorbed on Dowex 50, a strong cation exchanger, while In(III) and Sn(IV) were eluted [104]. Interestingly, Minami *et al.* found that Sb(V) went through a cation-exchange column in 0.2 M HCl whereas Te(IV) and Sn(IV) were adsorbed and later eluted with 0.5–1 M HCl [105].

4.2.5.   Radiochemical Separation of [119]Sb via a Dowex 1 Resin—With the help of a strong anion exchanger, Dowex 1, Smith and Reynolds were able to separate antimony, tin and tellurium from each other [106]. Sn, Sb and Te tracers in ~3 M HCl mixed with 0.1 M oxalic acid were loaded on columns of Dowex 1 (oxalate form). Tellurium was eluted with 0.1 M oxalic acid and antimony(V) with 0.1 M oxalic acid neutralised to pH 4.5. Tin(IV) was last eluted with 1 M sulphuric acid. Despite using a relatively long column (30 cm), cross contamination to the extent of about 1% was noted for both tin and antimony.

4.2.6.   Radiochemical Separation of [119]Sb via an Amberlite IRA-400 Resin— Many studies after Smith and Reynold's focused on the separation of Sb-Sn or Sb-Te binary mixtures. Dawson and Magee worked with another strong anion exchange resin, Amberlite IRA-400, attempting to separate tin and antimony [107]. The solution containing these two elements, ~2–3 M malonic acid and neutralised with 9 M ammonium hydroxide to pH 4.8, was transferred to the resin column. Antimony(V) was first eluted with 3% malonic acid adjusted to pH 4.8, followed by tin with 9 M sulphuric acid.

4.2.7. Radiochemical Separation of ^{119}Sb via an AN-31 and an AG 4-X4 Resin

—Maruyama and Yamaashi developed a simple method for the separation of carrier-free ^{125}Sb from neutron-irradiated tin [108]. The irradiated target was dissolved in concentrated HCl and diluted to 1 M HCl with water. Bromine was added into the solution to oxidise Sn(II) to Sn(IV) and Sb(III) to Sb(V), yielding a solution of 1 M HCl – 1 M HBr. Under such conditions, tin was strongly adsorbed by the strong anion exchange resin while antimony was not. In the final solution with a volume of 170 mL, a yield of ^{125}Sb of 90% and radiochemical purity of more than 99.99% were achieved.

Adopting the method presented by Maruyama and Yamaashi, Baluev *et al.* were able to reproduce the results using Dowex 1 [109]. Furthermore, in the latter study it was demonstrated that tin(IV) was eluted by 0.8 M HCl from an AN-31 anion exchange column while antimony(V) was afterwards washed out with 1 M HNO$_3$. The method with the use of a weak anion exchange resin for the separation of tin and antimony was also examined by Thisgaard and Jensen with radioactive material [55]. However, the results obtained by the latter researchers exhibit a reversed trend: antimony(V) was first eluted with 0.8 M HCl from the column containing the weakly basic anion exchange resin AG 4-X4. Such phenomena cause confusion as the two resins have similar functional groups. AN-31 is a weakly acidic anion exchanger which contains secondary and tertiary aliphatic amino groups serving as an active functional group [110], whereas AG 4-X4 resin has a tertiary amino functional group.

4.2.8. Radiochemical Separation of ^{119}Sb and ^{119}Te via a Dowex 1 Resin

—As ^{119}Sb may also be obtained by the decay of ^{119}Te, which can be produced by ^{nat}Sb(p,X)^{119}Te reactions [111, 112], it is necessary to introduce the separation of antimony-tellurium binary mixtures. Guin *et al.* reported a carrier-free separation of antimony from tellurium using a strong anion exchanger [113]. Antimony was oxidised to +5 oxidation state and taken up in 4 M HCl medium for loading onto the anion exchange resin, Dowex 1. The column was eluted with 3 M HCl and antimony activities were found to be eluted quantitatively. No tellurium activities were found in the eluted solution by examining its gamma-spectrum, indicating a separation of carrier-free antimony.

4.2.9. Radiochemical Separation of ^{119}Sb and ^{119}Te via a CL Resin, RE Resin, AG 1-X8 resin and Prefilter Resin

—Bennet *et al.* conducted a very detailed research aiming at enabling large-scale production of ^{119m}Te and ^{119}Sb for Auger radionuclide therapy [84]. The irradiated ^{nat}Sb target was dissolved in a mixture of 15.7 M HNO$_3$ and 28 M HF. To initiate the separation on CL resin, the solution matrix was converted to pure HF because presence of HNO$_3$ would lead to the leaching through of ^{119}Te. This solution was first passed through a column loaded with CL resin and ^{119m}Te was retained with the elution of ^{nat}Sb. To recover ^{119m}Te 10 M HNO$_3$ was used. After the initial separation, the eluate matrix was changed to 11.7 M HCl for a second Te/Sb separation. Loading this solution onto RE resin resulted into the retention of ^{119m}Te and partial elution of ^{nat}Sb. The former was eluted from the resin with water without the interference of antimony contents as this was confirmed by the use of ^{124}Sb tracer. In order to separate ^{119m}Te from the ^{nat}Sb target completely, the eluate comprising ^{119m}Te from the RE resin column was acidified to 2 M HCl, treated with H$_2$O$_2$, and transferred into an AG 1-X8 resin

column. Under these conditions ^{nat}Sb passed through the column; ^{119m}Te was retained, and subsequently eluted with H_2O. As a final step with the aim of removing organic impurities possibly introduced by the CL resin, the eluate obtained from the anion-exchange column was loaded directly onto Prefilter resin and ^{119m}Te eluted. The sulphur and phosphorous concentrations were below ~100 ppb for both elements examined by ICP-AES. Aside from the high purity of the final product, this method also features a relatively rapid separation (~36 h from target dissolution to final product suspension) compared to the half-lives of ^{119m}Te (4.7 d) [58] and ^{119}Sb (38.5 h) [58]. Moreover, this method is compatible with performing routine, large-scale production of ^{119m}Te and ^{119}Sb, which have the potential to meet the stringent Food and Drag Administration requirements for a ^{119m}Te/^{119}Sb active pharmaceutical ingredient.

4.2.10. Radiochemical Separation of ^{119}Sb via Solvent Extraction at TRIUMF and University of Wisconsin-Madison—At TRIUMF, the recovery of ^{119}Sb is achieved by solvent extraction, which initially was developed in collaboration with the Joint Institute for Nuclear Research (JINR) and further was adopted and optimized at TRIUMF and the University of Wisconsin. The irradiated natural tin target is dissolved in concentrated HCl. Presumably, all Sb(III) contents are oxidised to Sb(V) with the addition of 30% H_2O_2 for half an hour. Then an equal volume of dibutyl ether is added to the aqueous solution to extract antimony into the organic phase. The extract is washed with 10 M HCl twice while each washing step lasts for 30 minutes. Afterwards, Sb content is back-extracted to the aqueous phase by 0.1 M sodium citrate solution (pH 5.5). In each step of the separation, an aliquot is taken and later examined by gamma-spectrometry.

Using ^{120}Sb as the radioactive indicator and decay corrected, it is revealed that 84% of antimony contents are recovered in the final solution. Meanwhile, the activity of the tin isotope ^{117}Sn is not detected, from which it can be derived that Sb/Sn separation factor for this procedure is greater than 1000. Major losses of antimony contents occur during the back-extraction step. Minor losses are attributed to extraction and the two washing steps. Detailed separation procedures are currently in preparation in a separate manuscript.

5. COORDINATION CHEMISTRY OF $^{197M/G}$Hg AND ^{119}Sb

Due to residence in the organometallic family of the periodic table both mercury and antimony are capable of covalent bonding organic molecules. Though organometallics provide a unique opportunity in radiolabeling, especially when considering retention of small molecule geometries and binding properties, radiometal chelation is generally a choice route in radiometal radiopharmaceutical development, due to single step addition of radionuclide as a final step in radiopharmaceutical synthesis. For this purpose, a bifunctional chelator (BFC) is employed. Ideally, a BFC should be selective to the radiometal of choice at trace levels (pmol concentrations) while competing against mmol concentrations of other non-radioactive impurities. The radiometal-complex must be highly stable and inert, surviving *in vivo* competition against endogenous complexation agents such as various amino acids and glutathione. Furthermore, the BFC should exhibit fast complexation, incorporate an organic linker capable of functionalization to disease targeting moieities, have favorable biodistribution and be relatively inexpensive and straightforward to make

[1, 2]. Exploring the coordination chemistry of metal ions is essential for the proposal of an ideal chelator. We have included below a discussion of relevant literature for the non-radioactive metals, which may serve as a basis for BFC design in the radiopharmaceutical sciences. Significant room for scientific exploration exists in the field of radioantimony and radiomercury chelation for radiopharmaceutical application.

5.1. Chemistry of Mercury

5.1.1. In vivo Chemistry of Mercury—Mercury toxicity in humans leads to health effects on the central nervous, reproductive and cardiovascular system [114]; these effects are due to Hg's ability to form strong covalent bonds in biological systems and compete with essential metals in proteins. Metallothionein, a cysteine (sulfur) rich enzyme, is responsible for Hg^{2+} scavenging *in vivo* [115], and is believed to have a trigonal planer binding site that shows high affinity and selectivity for Hg^{2+} (stability constant of $4x10^5$) [116-118]. Glutathione is a low weight non-protein sulfhydryl-containing compound found in mammalian cells, which functions to trap and eliminate mercury from the body [119-121]. The formation constants ($\log\beta$) of these Hg^{2+} glutathione complexes have previously been reported in the literature to be 26.04 (0.95)[d] and 33.40 (1.03) [e]-41.58 for the [ML] and [M(L)$_2$] complexes, respectively [122, 123].

5.1.2. Complexation Chemistry of Mercury—Mercury (Hg) is a group 12 metal, which exists in two oxidation states Hg(I) and Hg(II) or in the elemental form of Hg, with Hg(II) (Hg^{2+}) being the most common in aqueous solution. In aqueous solutions, OH– and Cl– ligands are commonly found complexed with Hg^{2+}, when hydrosulfide (SH-) or thiolate (SR-) ligands are absent [124]. Hg^{2+} is classified as a soft metal, according to Pearson's hard-soft acid-base (HSAB) theory [125, 126]. An intrinsic property of soft acids, such as Hg^{2+}, is that they are highly polarizable and will preferentially bind to ligands with soft bases such as sulphur (S-), phosphorous (P-), tellurium (Te-) and selenium (Se-) through covalent interactions [127-134]. Nitrogen (N-) has also been seen to bind to Hg^{2+} regardless of its hard acid-like character [135-138]. Hg^{2+} forms stronger bonds with S-, P- and N-compared to any other divalent metal [134].

With a spherical d^{10} electron configuration, Hg^{2+} is associated with a flexible coordination environment and the geometries of formed complexes can vary greatly, with significant distortions being common [134, 139]. Interestingly, due to the lack of preferential binding, large coordination diameter (CN 6: 102 pm, CN 4: 96 pm, CN 8:114 pm) and rapid ligand exchange, Hg^{2+} exhibits several different coordination numbers and geometries when bound to the same ligands [140]. Monodentate ligands generally form a linear geometry with atoms that have more ionic character (*i.e.,* oxygen), whereas a tetrahedral geometry is favoured with covalent character bonding atoms (*i.e.,* sulfur and iodine); however, multidentate ligands open up a broad range of possible geometries [124, 141]. Reported Hg^{2+} complexes that have a coordination number of six or higher are less common compared to other metals, but their discovery is becoming more frequent [134, 142-147].

Studies of polythioether crown Hg^{2+} exhibit rare geometries of the Hg^{2+} ion (*i.e.* square planar, square pyramidal and octahedral) due to the high binding affinity of the sulfur donor

atoms [134]. Octahedral complexes, when observed, usually form a distorted complex with two relatively short bonds and four longer bonds [124, 134]. Due to the lack of preference for a specific coordination number or geometry, it is critical to determine the structural characteristics of a Hg^{2+} complex through X-ray crystallography [124]. Past studies have focused on the structural and crystallography data of mercury to determine the association between the coordination number, ligand donor atoms, bond length and bond angles to the specific isomer of the complex [141].

Both cyclic and acyclic sulfur-rich ligands have been studied to determine the binding properties of Hg^{2+}. However, studies indicate that the macrocyclic effect of the thiocrown ethers only show effects when the ring size is large and flexible enough to contain the Hg^{2+} atom [148]. As such, Hg^{2+} has shown a higher affinity for sulfur-rich acyclic ligands compared to smaller cyclic macrocycles (Fig. 9) [148, 149]. When polythioethers are large enough to display the macrocyclic effect there is a reduction of the exchange process, which occurs with the labile Hg^{2+} metal ion, leading to an increase in the kinetic inertness of the complex [134].

5.2. Mercury Chelating Ligands

Previous development of bifunctional chelators (BFCs) for $^{197m/g}Hg$ radiopharmaceuticals is limited. To our knowledge, from the time of writing, one account utilizing a BFC for $^{197/m}Hg$ radiolabeling has been reported (Fig. 10) [150]. The trithiamacrocycle was conjugated to a covalent linker for the use of antibody attachment by the activated ester. This bifunctional chelator labeled with $^{197m/g}Hg$ was conjugated to immunoglobulin (rabbit IgG) by ammonolysis. The bioconjugate was stable in buffered saline for a minimum of 24 hours, while the stability during the incubation in serum exhibited some loss of radiolabelling. The authors suggested the chelator to be a viable approach to radiolabel antibodies with soft radiometals.

5.2.1.   . Mercury Environmental Sensing Ligands—As a result of Hg^{2+} compounds threatening human life, a series of water-soluble extraction ligands have been synthesized for selective and sensitive Hg^{2+} detection [151]. Thiocrowns have been studied to selectively recover Hg^{2+} for extraction from a polar to non-polar phase. Macrocycles containing thiocarbonyls have been used to successfully achieve recovery where the thiocarbonyls are responsible for the strong complexation of the Hg^{2+} ions, allowing for selective binding of Hg^{2+} over other metals such as copper [152]. Further, a pendant crown thioether developed by Baumann and Reynolds was used for extraction of >99% of Hg^{2+} in acidic aqueous solutions [153].

Many fluorescent probes have been synthesized and studied as a tool to determine the Hg^{2+} content of different water supplies/sources as well as visualizing the Hg^{2+} content in living cells [114]. These fluorescent probes are conjugated to a chelator that has high sensitivity and selectivity for Hg^{2+} in solution, proving detection of low concentrations and resulting in a 1:1 stoichiometry with Hg^{2+} [154]. These Hg^{2+} chelators contain a wide range of donor atoms, for example, Se-, N-, O- and/or S- atoms along with alkene and/or alkyne moieties [155-158]. These binding atoms have been introduced into the probes as derivatized

dithia-dioxa-aza macrocycles, thia-aza crown, thioether crowns, oxa-aza crowns, porphyrin rings, calixarene, aza-oxa cryptands and acyclic arms or small molecules (Fig. 11) [154, 156, 157, 159-166].

Gold nanoparticles have been used for mercury sensing probes in the environment as a cheap and easy detection method exhibiting a high affinity for Hg^{2+} at low concentrations [167-171]. These particles are either functionalized with moieties, which possess an affinity for Hg^{2+} (*i.e.,* sulfur) or non-functionalized, as mercury's unique chemical and physical properties enable it to amalgamate, forming strong metallic bonds with metals such as gold, silver, copper, indium, tin and zinc [172].

5.2.2. . Chelating Ligands for Mercury Poisoning—Chelators for the treatment of Hg^{2+} poisoning possess a high affinity to the metal compared to endogenous ligands. These ligands tend to have a high-water solubility to increase excretion through the kidneys. Current ligands used for Hg^{2+} poisoning are dimercaprol (2,3-Dimercaptopropanol/British Anti Lewisite, BAL), 2,3-Dimercaptosuccinic acid (DMSA), D-penicillamine (DPEN) and 2,3-Dimercapto-1-propanesulfonic acid (DMPS), the associated stability constants (logβ) of the Hg^{2+} complexes [HgL] can be found in Table 6 [173-178]. More recently, DMPS has increased in popularity as it is found to have higher sensitivity for lower levels of Hg^{2+} and is found to be less toxic as it does not cross the blood-brain barrier [179].

5.3. Mercury-197's Previous Applications

In the early 1960s, ^{203}Hg ($t_{1/2}$ = 46.6 days, β− (100%), γ ($E_γ$ 279 keV, $I_γ$ = 82%)) was the main isotope incorporated into chlormerodrin (3-chloromercury-2-methoxyprop-1-yl) (Fig. 12), a water-soluble SPECT imaging agent [180]. Though advantages of using $^{197m/g}Hg$ over ^{203}Hg include having a shorter half-life, a greater number of useful gamma-ray emissions and a lower renal dose allowing for the ability to administer a higher dose to a patient, at the time $^{197m/g}Hg$ could not be produced in a high specific activity which leads to mercury poisoning and precluded the use of this isotope. In 1966, once isotope production issues were mitigated, $^{197m/g}Hg$-labeled chlormerodrin increased in popularity [181], and the use of $^{197m/g}Hg$ for brain, kidney and spleen imaging increased [181-184]. Nonetheless, this radiopharmaceutical was only in use until the 1970s, before it was replaced with Techicium-99m (^{99m}Tc) imaging agents [181]. In the 1970s, $^{197m/g}Hg$-labeled human lymphocytes were synthesised to study their migration pattern. Lymphocyte labeling was done in various physicochemical conditions, additionally, the subcellular distribution of $^{197m/g}HgCl_2$ within the cell was established, which showed 60% of the tracer was localized within the nucleus and cellular membrane while the remaining was found in the mitochondria and microsomes [185]. $^{197m/g}Hg$ had shown to possess useful radiation characteristics and favorable chemical properties for radiolabeling compared to previously studied radiometals. Due to the limited exploration of $^{197m/g}Hg$ in radiopharmaceuticals, there lies room for improvement and development for this theranostic metal.

5.4. Chemistry of Antimony

Being a group 15 organometallic element with ground-state electron configuration $[Kr]4d^{10}5s^25p^3$, antimony has two main oxidation states, Sb(III) and Sb(IV) [186], but some

antimony ores, such as breithauptite NiSb, have a negative oxidation state [187]. The most common coordination numbers are 3, 4, 5, and 6 [187, 188] and frequently encountered geometries are shown within Fig. 13. With ionic atomic radii of 76 pm for Sb(III), 60 pm Sb(V) [186, 187] and electric polarizability reported to be 42.61-44.57 (depending on computational method) [189, 190], Sb is a large, soft metal.

5.5. Organometallic Compounds of Antimony

An emergent interest in organoantimony molecules has led to a recent increase in the publication of stilbene molecules and chemical synthesis. Though unstable and susceptible to hydrolysis, antimony(III)-nitrogen species are known, an example being $[(PNR)_2(NR)_2Sb]Cl$, a polycyclic cage complex with antimony bonded to one chlorine and three nitrogen atoms [187]. Anionic compounds with antimony-phosphorus bonds have been reported, such as the diphospha-substituted antimonide $C_6H_4P_2Sb^-$ (Fig. 14 upper left) [187]. Many examples of Sb-C bonded molecules exist within the literature [191]. The acyclic system 2-stiba-1,3--dionato ligand (Fig. 14 upper right) has been reported to contain delocalized Sb=C, with length 2.15 Å, a bond length within the normal single-bonded range [191]. In rare instances, Sb=C bonded molecules have been reported, one example being 2,3-distibabutadiene (Fig. 14 bottom left), and have been found to be thermally stable to temperatures above 200 °C, an impressive feature [191]. Antimony can form catenated complexes, such as $[(Bu^tP)_3Sb-Sb(PBu^t)_3]_2$ (Fig. 14 bottom right), however, with Sb-Sb single-bond energy of 128 kJ/mol, antimony compounds are rather weak [192].

5.6. *In vivo* Cchemistry of Antimony

Antimony-based complexes are used in the treatment of multiple parasitic infections as pentavalent Sb (*e.g.* sodium stibogluconate and meglumine antimoniate shown in Fig. 15) is used clinically in the treatment of leishmaniasis [193]. After reduction of Sb(V) to Sb(III) inside of the parasite, Sb(III) interferes with the parasite's thiol redox metabolism, effluxing trypanothione and glutathione from the cell and inhibiting trypanothione reductase enzymatic activity [194].

Interaction of antimony with biological molecules provides supporting evidence toward the strong interaction of Sb with thiol donor atoms. Due to this proposed mechanism of action, anti-tumor properties of Sb(III) and Sb(V) compounds (studied in DTPA and thiol coordinated systems) have drawn interest [195, 196] toward the development of new monodentate thiol complexes [197].

Though a choice chelator for Sb has yet to be developed and publicized, help can be drawn from work chelating similar elements, such as fellow pnicogen arsenic [186]. 2,3-dimercaptopropane-1-sulfonic acid (DMPS) and meso-2,3-dimercaptosuccinic acid (DMSA) are chelators used clinically in the removal of arsenic and antimony from individuals being treated for heavy metal poisoning [198]. Additionally, antimony has proven itself thiophilic, forming many complexes with thiol ligands containing sulfur donor atoms [197, 199-202]. Recent developments in thiol chelation of radioarsenic and antimony's proven history of thiophilicity provide promise in future antimony bifunctional chelation [203-205].

5.7. Antimony Chelation

Potassium antimonyl tartrate (Fig. 15) historically was used in treatment for the parasitic infection Schistosoma [206]. The first and only reported chelation of radioantimony was Thakur's report of [117]Sb Potassium Antimonyl Tartrate (PAT) in 1969. The authors prepare PAT samples free from contamination and suitable for injection [207]. However, no mention of specific activity or radio complex stability is included. Within this bidentate ligand complex, two Sb(III) atoms are buried within eight oxygen atoms, each metal ion forming four coordination bonds. Though insightful into the coordination environment, which can stabilize Sb, a chelator suitable for organic linking to targeting vector is required to provide radiopharmaceutical selectivity.

6. DISCUSSION

MAE emitters are attractive for application in cancer therapy as their emissions are highly cytotoxic when deposited close to the cellular DNA. There has been an increased interest in these emitters for therapeutic uses, specifically for micrometastatic and small undetectable tumours, as the short path-length and high LET of MAEs result in minimal toxicity to surrounding healthy tissue and strong tumour growth inhibition. Although these radionuclides show promising therapeutic applications for incorporation into radiopharmaceuticals, very few clinical applications have been presented to date.

For the success of Targeted Auger Therapy, it is necessary to establish the production of radionuclides, which are practically suitable for Auger therapy. The impact of other emissions (*e.g.,* photons or betas) should be accounted for in dosimetry considerations (*e.g.,* [111]In); moreover, the proposed nuclide should have a suitable half-life compatible with the biological half-lives of common delivery systems used in radiopharmaceuticals. Another important criterion for the suitability of Auger emitters for Targeted Therapy is the possibility of producing isotope with high specific (and molar) activity and radionuclidic purity; this is necessary to enable incorporation of sufficient therapeutic doses into delivery systems (*e.g.,* peptides or nanotransporters).

Many research candidates for Auger therapy are metals that are rarely used in nuclear medicine, therefore developing stable chelation strategies is another key component for the development of Auger-emitting radiopharmaceuticals. In addition, testing available delivery systems *in vitro* and *in vivo* is key for determining a combination of isotopes and biomolecules, as some Auger emitters may be efficient at causing cytotoxic effects when located outside of the cell nucleus.

In the present review, two promising candidates for Auger therapy are discussed, namely [119]Sb and [197]Hg. By their decay characteristics, antimony−[119sb] is superior to [197]Hg and possibly one of the most suitable candidates for Auger therapy when delivered near DNA. However, the absence of well-established delivery systems (chelator+ targeting vector) and challenges with production of high specific activity and radionuclidic pure antimony−[119sb] have precluded demonstrated potential thus far. On the other hand, [197]Hg can be relatively easy to produce with satisfactory yields and purity for applications and can allow dosimetry studies. Notably, mercury−[197Hg] possesses a metastable and ground state; the ground state

emits decays suitable for Auger therapy, while the metastable form emits gamma rays well suited for SPECT imaging. For Auger therapy applications the amount of metastable mercury should be minimized through decay or viable production routes.

From isotope production and radiochemistry aspects at TRIUMF, we were able to establish routine production of pre-clinical quantities of $^{197m/8}$Hg (100's MBq/per production) by adopting a previously reported separation technique based on LN resin to separate no carrier added (nca) mercury from mg's of gold target material. Currently, several potential chelators synthesized in the Ramogida lab are being tested. Additionally, in collaboration with the Reilly lab at University of Toronto (Canada), the *in vitro* toxicity of ^{197g}Hg is being investigated. For the future development, our team is planning to establish a better strategy for characterizing produced mercury isotopes and ratios between metastable and ground states through gamma spectroscopy. We are also looking into alternative strategies for separation of mercury from gold by finding sorbents which will retain Hg over Au and by adding additional column-based separation steps to avoid a final evaporation step for mercury radiolabelling preconditioning.

For production of ^{119}Sb, irradiation of natural tin is performed at TRIUMF to obtain radiotracers of Sb and Sn for chemistry development and chelation, while the University of Wisconsin-Madison is implementing enriched tin-119 to produce isotopically pure ^{119}Sb. In collaboration with the radiochemistry group at Joint Institute for Nuclear Research (JINR) in Dubna, we developed a liquid-liquid extraction procedure for radiochemical isolation of nca antimony from mg's of tin using ethers or ketones; further method optimization is ongoing in collaboration with TRIUMF and the University of Wisconsin-Madison. Continued production optimization includes irradiation of enriched tin-119, transferring radiochemical separation into synthesized ether/ketone resins for column-based chromatography, and pursuing indirect production *via* the p,3n reaction on Sb for production of ^{119}Te/^{119}Sb generator.

CONCLUSION

Both $^{197m/g}$Hg and ^{119}Sb are two such radionuclides that have high potential in MAE targeted therapy. Further developments in their production, radiochemical purification, and chelation are required to leverage these isotopes successfully in radiopharmaceutical design. In particular, the development of a specific, selective chelator with properties suitable for radiopharmaceutical elaboration will allow for *in vivo* exploration of the therapeutic efficacy of these unique radionuclides.

ACKNOWLEDGEMENTS

REFERENCES

[1]. Price EW; Orvig C Matching chelators to radiometals for radiopharmaceuticals. Chem. Soc. Rev, 2014, 43(1), 260–290. 10.1039/C3CS60304K [PubMed: 24173525]

[2]. Ramogida CF; Orvig C Tumour targeting with radiometals for diagnosis and therapy. Chem. Commun. (Camb.), 2013, 49(42), 4720–4739. 10.1039/c3cc41554f [PubMed: 23599005]

[3]. Boros E; Packard AB Radioactive Transition Metals for Imaging and Therapy. Chem. Rev, 2019,119(2), 870–901. 10.1021/acs.chemrev.8b00281 [PubMed: 30299088]

[4]. Bavelaar BM; Lee BQ; Gill MR; Falzone N; Vallis KA Subcellular Targeting of Theranostic Radionuclides. Front. Pharmacol, 2018, 9(9), 996. 10.3389/fphar.2018.00996 [PubMed: 30233374]

[5]. Li T; Ao ECI; Lambert B; Brans B; Vandenberghe S; Mok GSP Quantitative Imaging for Targeted Radionuclide Therapy Dosimetry - Technical Review. Theranostics, 2017, 7(18), 4551–4565. 10.7150/thno.19782 [PubMed: 29158844]

[6]. Qaim SM; Scholten B; Neumaier B New Developments in the Production of Theranostic Pairs of Radionuclides. J. Radioanal. Nucl. Chem, 2018, 318(3), 1493–1509. 10.1007/s10967-018-6238-x

[7]. Karimi Z; Sadeghi M; Mataji-Kojouri N ^{64}Cu, a powerful positron emitter for immunoimaging and theranostic: Production *via* ^{nat}ZnO and ^{nat}ZnO-NPs. Appl. Radiat. Isot, 2018, 137, 56–61. 10.1016/j.apradiso.2018.03.007 [PubMed: 29571037]

[8]. Pandit-Taskar N Targeted Radioimmunotherapy and Theranostics with Alpha Emitters. J. Med. Imaging Radiat. Sci, 2019, 50(4)(Suppl. 1), S41–S44. 10.1016/jjmir.2019.07.006 [PubMed: 31451417]

[9]. Lau J; Lin KS; Bénard F Past, Present, and Future: Development of Theranostic Agents Targeting Carbonic Anhydrase IX. Theranostics, 2017, 7(17), 4322–4339. 10.7150/thno.21848 [PubMed: 29158829]

[10]. Thorp-Greenwood FL; Coogan MP Multimodal radio-(PET/SPECT) and fluorescence imaging agents based on metallo-radioisotopes: current applications and prospects for development of new agents. Dalton Trans., 2011, 40(23), 6129–6143. 10.1039/c0dt01398f [PubMed: 21225080]

[11]. Cornelissen B Imaging the inside of a tumour: a review of radionuclide imaging and theranostics targeting intracellular epitopes. J. Labelled Comp. Radiopharm, 2014, 57(4), 310–316. 10.1002/jlcr.3152 [PubMed: 24395330]

[12]. Auger P The Auger Effect. Surf. Sci, 1975, 48(1), 1–8. 10.1016/0039-6028(75)90306-4

[13]. Meitner L Über Die Entstehung Der β-Strahl-Spektren Radioaktiver Substanzen. Z. Phys, 1922, 9(1), 131–144. 10.1007/BF01326962

[14]. Duparc OH; Meitner L; Ellis CD Pierre Auger – Lise Meitner: Comparative Contributions to the Auger Effect. Int. J. Mater. Res, 2009, 100(9), 1162–1116. 10.3139/146.110163

[15]. O'Donoghue JA; Wheldon TE Targeted radiotherapy using Auger electron emitters. Phys. Med. Biol, 1996, 41(10), 1973–1992.https://doi.org/https://doi-org.proxy.lib.utk.edu/10.1088/0031-9155/41/10/005http://dx.doi.org/10.1088/0031-9155/41/10/009http://dx.doi.org/10.1088/0031-9155/41/10/009 [PubMed: 8912375]

[16]. Cornelissen B; Vallis KA Targeting the nucleus: an overview of Auger-electron radionuclide therapy. Curr. Drug Discov. Technol, 2010, 7(4), 263–279. 10.2174/157016310793360657 [PubMed: 21034408]

[17]. Humm JL; Howell RW; Rao DV Dosimetry of Auger-electron-emitting radionuclides: report no. 3 of AAPM Nuclear Medicine Task Group No. 6. Med. Phys, 1994, 21(12), 1901–1915. 10.1118/L597227 [PubMed: 7700197]

[18]. Freudenberg R; Apolle R; Walther M; Hartmann H; Kotzerke J Molecular imaging using the theranostic agent $^{197(m)}$Hg: phantom measurements and Monte Carlo simulations. EJNMMI Phys., 2018, 5(1), 15. 10.1186/s40658-018-0216-9 [PubMed: 30146662]

[19]. Kassis AI Molecular and cellular radiobiological effects of Auger emitting radionuclides. Radiat. Prot. Dosimetry, 2011, 143(2-4), 241–247. 10.1093/rpd/ncq385 [PubMed: 21106639]

[20]. Goddu SM; Howell RW; Rao DV Calculation of equivalent dose for Auger electron emitting radionuclides distributed in human organs. Acta Oncol., 1996, 35(7), 909–916. 10.3109/02841869609104045 [PubMed: 9004771]

[21]. Faraggi M; Gardin I; de Labriolle-Vaylet C; Moretti JL; Bok BD The influence of tracer localization on the electron dose rate delivered to the cell nucleus. J. Nucl. Med, 1994, 35(1), 113–119. [PubMed: 8271031]

[22]. Hofer KG Biophysical aspects of Auger processes--A review. Acta Oncol, 1996, 35(7), 789–796. 10.3109/02841869609104028 [PubMed: 9004754]

[23]. Pouget J-P; Santoro L; Raymond L; Chouin N; Bardiès M; Bascoul-Mollevi C; Huguet H; Azria D; Kotzki P-O; Pèlegrin M; Vivès E; Pèlegrin A Cell membrane is a more sensitive target than cytoplasm to dense ionization produced by auger electrons. Radiat. Res, 2008, 170(2), 192–200. 10.1667/RR1359.1 [PubMed: 18666820]

[24]. Saha G Fundamentals of Nuclear Pharmacy, 2013, 53 10.1017/CB09781107415324.004

[25]. Pouget JP; Navarro-Teulon I; Bardiès M; Chouin N; Cartron G; Pèlegrin A; Azria D Clinical radioimmunotherapy--the role of radiobiology. Nat. Rev. Clin. Oncol, 2011, 8(12), 720–734. 10.1038/nrclinonc.2011.160 [PubMed: 22064461]

[26]. Chakravarty N; Rattan SS; Singh RJ; Ramaswami A Decay Studies of 197T1 (2.84 H) and 197mHg (23.8 H). Radiochim. Acta, 1993, 61(1), 9–14. 10.1524/ract.1993.61.l.9

[27]. Adelstein SJ; Kassis AI Strand breaks in plasmid DNA following positional changes of Auger-electron-emitting radionuclides. Acta Oncol., 1996, 35(7), 797–801. 10.3109/02841869609104029 [PubMed: 9004755]

[28]. Chan PC; Lisco E; Lisco H; Adelstein SJ The radiotoxicity of iodine-125 in mammalian cells II. A comparative study on cell survival and cytogenetic responses to 125IUdR, 131TUdR, and 3HTdR. Radiat. Res, 1976, 67(2), 332–343. 10.2307/3574422 [PubMed: 948559]

[29]. Howell RW; Rao DV; Hou DY; Narra VR; Sastry KS The question of relative biological effectiveness and quality factor for auger emitters incorporated into proliferating mammalian cells. Radiat. Res, 1991, 128(3), 282–292. 10.2307/3578051 [PubMed: 1961925]

[30]. Narra VR; Howell RW; Harapanhalli RS; Sastry KSR; Rao DV Radiotoxicity of some iodine-123, iodine-125 and iodine-131-labeled compounds in mouse testes: implications for radiopharmaceutical design. J. Nucl. Med, 1992, 33(12), 2196–2201. [PubMed: 1460515]

[31]. Snelling L; Miyamoto CT; Bender H; Brady LW; Steplewski Z; Class R; Emrich J; Rackover MA Epidermal growth factor receptor 425 monoclonal antibodies radiolabeled with iodine-125 in the adjuvant treatment of high-grade astrocytomas. Hybridoma, 1995,14(2), 111–114. 10.1089/hyb.1995.14.111 [PubMed: 7590764]

[32]. Aronsson EF; Grétarsdóttir J; Jacobsson L; Bäck T; Hertzman S; Lindegren S; Karlsson B; Lindholm L; Holmberg S; Hafström L; Mattsson S Therapy with 125I-labelled internalized and non-internalized monoclonal antibodies in nude mice with human colon carcinoma xenografts. Nucl. Med. Biol, 1993, 20(2), 133–144. 10.1016/0969-8051(93)90105-4 [PubMed: 8448565]

[33]. Volkert WA; Goeckeler WF; Ehrhardt GJ; Ketring AR Therapeutic radionuclides: production and decay property considerations. J. Nucl. Med, 1991, 32(1), 174–185. [PubMed: 1988628]

[34]. Walther M; Preusche S; Bartel S; Wunderlich G; Freudenberg R; Steinbach J; Pietzsch HJ Theranostic mercury: (197(m))Hg with high specific activity for imaging and therapy. Appl. Radiat. Isot, 2015, 97, 177–181. 10.1016/j.apradiso.2015.01.001 [PubMed: 25588997]

[35]. Lebeda O; ervenák J Nuclear Inst. and Methods in Physics Research B Revised Cross-Sections for Formation of Theranostic Deuteron-Induced Reactions on 197 Au Hg in Proton- And. Nucl. Instrum. Methods Rhys. Res. B, 2020, 478(5), 85–91. 10.1016/j.nimb.2020.05.014

[36]. Lebeda O; Kondev FG; ervenák J Branching Ratio and γ-Ray Emission Probabilities in the Decay of the $J\pi$=13/2+ Isomer in 197Hg. Nucl. Instruments Methods Phys. Res. Sect. A Accel. Spectrometers. Detect. Assoc. Equip, 2019, 2020(959)163481 10.1016/j.nima.2020.163481

[37]. Huang X; Zhou C Nuclear Data Sheets for A = 197. Nucl. Data Sheets (N.Y. N.Y.), 2005, 104(2), 283–426. 10.1016/j.nds.2005.01.001

[38]. Rosemer J Radiochemistry of Mercury*National Research Council*, The National Academies Press.: Washington, DC, 1970.

[39]. Ku A; Facca VJ; Cai Z; Reilly RM Auger electrons for cancer therapy - a review. EJNMMI Radiopharm Chem, 2019, 4(1), 27. 10.1186/s41181-019-0075-2 [PubMed: 31659527]

[40]. Rosenkranz AA; Slastnikova TA; Karmakova TA; Vorontsova MS; Morozova NB; Petriev VM; Abrosimov AS; Khramtsov YV; Lupanova TN; Ulasov AN.; Yakubovskaya RI; Georgiev GP; Sobolev AS Antitumor Activity of Auger Electron Emitter [111]In Delivered by Modular Nanotransporter for Treatment of Bladder Cancer With EGFR Overexpression. Front. Pharmacol, 2018, 9(NOV), 1331. 10.3389/fphar.2018.01331 [PubMed: 30510514]

[41]. Canada Health. Mercury. 1986.

[42]. Wong SL; Lye EJD Lead, mercury and cadmium levels in Canadians. Health Rep., 2008, 19(4), 31–36.

[43]. U.S. Centers for Disease Control and Prevention. The Fourth National Report on Human Exposure to Environmental Chemicals, 2015.

[44]. Becker K; Schulz C; Kaus S; Seiwert M; Seifert B German Environmental Survey 1998 (GerES III): environmental pollutants in the urine of the German population. Int. J. Hyg. Environ. Health, 2003, 206(1), 15–24. 10.1078/1438-4639-00188 [PubMed: 12621899]

[45]. Schmitz W Exposure of Children. Encycl. Anc. Hist, 2012.

[46]. Watson I National Poisons Information Service; Association of Clinical Biochemists. Laboratory analyses for poisoned patients: joint position paper. Ann. Clin. Biochem, 2002, 39(Pt 4), 328–339. 10.1258/000456302760042083 [PubMed: 12117436]

[47]. Brodkin E; Copes R; Mattman A; Kennedy J; Kling R; Yassi A Lead and mercury exposures: interpretation and action. CMAJ, 2007, 176(1), 59–63. 10.1503/cmaj.060790 [PubMed: 17200393]

[48]. Rahmim A; Zaidi H PET versus SPECT: strengths, limitations and challenges. Nucl. Med. Commun, 2008, 29(3), 193–207. 10.1097/MNM.0b013e3282f3a515 [PubMed: 18349789]

[49]. Mountz JM Gamuts in Nuclear Medicine*Clin. Nucl. Med*, Second Edition;, 1990, 15, pp. (1)58–59.

[50]. Grünberg J; Lindenblatt D; Dorrer H; Cohrs S; Zhemosekov K; Köster U; Türler A; Fischer E; Schibli R Anti-L1CAM radioimmunotherapy is more effective with the radiolanthanide terbium-161 compared to lutetium-177 in an ovarian cancer model. Eur. J. Nucl. Med. Mol. Imaging, 2014, 41(10), 1907–1915. 10.1007/s00259-014-2798-3 [PubMed: 24859811]

[51]. Center NND Nuclear Structure and Decay Data: NuDat 2.7,

[52]. Symochko DM; Berkeley L; Tuli JK Nuclear Data Sheets for A = 119 *. Nucl. Data Sheets (N.Y. N.Y.), 2009, 110(11), 2945–3105. 10.1016/j.nds.2009.10.003

[53]. Eckerman KF; Endo A MIRD: Radionuclide Data and Decay Schemes, 2nd ed; Society of Nuclear Medicine, 2008.

[54]. Bernhardt P; Forssell-Aronsson E; Jacobsson L; Skarnemark G Low-energy electron emitters for targeted radiotherapy of small tumours. Acta Oncol., 2001, 40(5), 602–608. 10.1080/028418601750444141 [PubMed: 11669332]

[55]. Thisgaard H; Jensen M 119Sb--a potent Auger emitter for targeted radionuclide therapy. Med. Rhys, 2008, 35(9), 3839–3846. 10.1118/l.2963993

[56]. Hsiao YY; Hung TH; Tu SJ; Tung CJ Fast Monte Carlo simulation of DNA damage induction by Auger-electron emission. Int. J. Radiat. Biol, 2014, 90(5), 392–400. 10.3109/09553002.2014.892649 [PubMed: 24517473]

[57]. Falzone N; Femández-Varea JM; Flux G; Vallis KA Monte Carlo Evaluation of Auger Electron-Emitting Theranostic Radionuclides. J. Nucl. Med, 2015, 56(9), 1441–1446. 10.2967/jnumed.114.153502 [PubMed: 26205298]

[58]. Sóti Z; Magill J; Dreher R Karlsruhe Nuclide Chart – New 10th Edition.EPJ Nucl. Sci. Technol; , 2019.

[59]. Elmaghraby EK; Hassan KF; Omara H; Saleh ZA Production of the mercury-197 through proton induced reaction on gold. Appl. Radiat. Isot, 2010, 68(9), 1694–1698. 10.1016/j.apradiso.2010.04.009 [PubMed: 20418105]

[60]. Overton MC III; Haynie TP; Snodgrass SR Brain Scans in Nonneoplastic Intracranial Lesions: Scanning With Chlormerodrin Hg 203 and Chlormerodrin Hg 197. JAMA, 1965, 191(6), 431–436. 10.1001/jama.1965.03080060005001 [PubMed: 14238022]

[61]. Hansen LF; Jopson RC; Mark H; Swift CD Ta181(p, n)W181 and Au197(p, n)Hg197 Excitation Functions between 4 and 13 MeV. Nucl. Phys, 1962, 30(C), 389–398. 10.1016/0029-5582(62)90062-7

[62]. Ribeiro Guevara S; Žižek S; Repinc U; Pérez Catán S; Jaćimović R; Horvat M Novel methodology for the study of mercury methylation and reduction in sediments and water using 197Hg radiotracer. Anal. Bioanal. Chem, 2007, 387(6), 2185–2197. 10.1007/s00216-006-1040-y [PubMed: 17205268]

[63]. Gloris M; Michel R; Sudbrock F; Herpers U; Malmborg P; Holmqvist B Proton-Induced Production of Residual Radionuclides in Lead at Intermediate Energies. Nucl. Instruments Methods Phys. Res. Sect. A Accel. Spectrometers. Detect. Assoc. Equip, 2001, 463(3), 593–633. 10.1016/S0168-9002(01)00174-7

[64]. Ziegler JF; Ziegler MD; Biersack JP SRIM - The Stopping and Range of Ions in Matter (2010). Nucl. Instruments Methods Phys. Res. Sect. B Beam Interact. with Mater. Atoms, 2010, 268(11–12), 1818–1823. 10.1016/j.nimb.2010.02.091

[65]. Zeisler S; Clarke B; Kumlin J; Hook B; Varah S; Hoehr C A Compact Quick-Release Solid Target System for the TRIUMF TR13 Cyclotron. Instruments, 2019, 3(1), 16. 10.3390/instruments3010016

[66]. Hoehr C; Oehlke E; Benard F; Lee CJ; Hou X; Badesso B; Ferguson S; Miao Q; Yang H; Buckley K; Hanemaayer V; Zeisler S; Ruth T; Celler A; Schaffer P (44g)Sc production using a water target on a 13MeV cyclotron. Nucl. Med. Biol, 2014, 41(5), 401–406. 10.1016/j.nucmedbio.2013.12.016 [PubMed: 24513279]

[67]. Oehlke E; Hoehr C; Hou X; Hanemaayer V; Zeisler S; Adam MJ; Ruth TJ; Celler A; Buckley K; Benard F; Schaffer P Production of Y-86 and other radiometals for research purposes using a solution target system. Nucl. Med. Biol, 2015, 42(11), 842–849. 10.1016/j.nucmedbio.2015.06.005 [PubMed: 26264926]

[68]. Agency IAE Gallium-68 Cyclotron Production; Vienna, 2019.

[69]. Hoehr C; Morley T; Buckley K; Trinczek M; Hanemaayer V; Schaffer P; Ruth T; Bénard F Radiometals from liquid targets: 94mTc production using a standard water target on a 13 MeV cyclotron. Appl. Radiat. Isot, 2012, 70(10), 2308–2312. 10.1016/j.apradiso.2012.06.004 [PubMed: 22871432]

[70]. Vogg A; Lang R; Meier-Böke P; Scheel W; Reske S; Neumaier B Cyclotron Production of Radionuclides in Aqueous Target Matrices as Alternative to Solid State Targetry: Production of Y-86 as Example. 6th Int. Conf. Nucl. Radiochem., 20042014.

[71]. Raslis J; Lebeda O; Kucera J Liquid Target System for Production of 86Y. The 13th international workshop on targetry and target chemistry proceedings, Denmark2011, 1787, pp. 234–239.

[72]. Pandey MK; Byrne JF; Jiang H; Packard AB; DeGrado TR Cyclotron production of (68)Ga *via* the (68)Zn(p,n)(68)Ga reaction in aqueous solution. Am. J. Nucl. Med. Mol. Imaging, 2014, 4(4), 303–310. [PubMed: 24982816]

[73]. Jensen M; Clark J Direct Production of Ga-68 from Proton Bombardment of Concentrated Aqueous Solutions of [Zn-68] Zinc Chloride. Mikael The 13th international workshop on targetry and target chemistry proceedings, 2011, p. 052.

[74]. Alves F; Alves VHP; Do Carmo SJC; Neves ACB; Silva M; Abrunhosa AJ Production of Copper-64 and Gallium-68 with a Medical Cyclotron Using Liquid Targets. Mod. Phys. Lett. A, 2017, 32(17), 1–21. 10.1142/S0217732317400132

[75]. Dias GM; Ramogida CF; Rousseau J; Zacchia NA; Hoehr C; Schaffer P; Lin KS; Bénard F Peptide Radiolabelling and in Vivo Imaging Using Ga-68 Directly Produced in Liquid Targets.Journal of Labelled Compounds and Radiopharmaceuticals; Elsevier Inc., 2017, Vol. 60, p. 400.

[76]. Li K; Jahangiri P; Zacchia N; Uittenbosch T; Buckley K Modular Design for a Liquid Target., 2017, 020013 10.1063/L4983544

[77]. Pritychenko B; Sonzogni A Q-Value Calculator (QCalc). National Nuclear Data Center, Brookhaven National Laboratory,

[78]. Thisgaard H; Jensen M; Elema DR Medium to large scale radioisotope production for targeted radiotherapy using a small PET cyclotron. Appl. Radiat. Isot, 2011, 69(1), 1–7. 10.1016/j.apradiso.2010.07.019 [PubMed: 20724171]

[79]. Thisgaard H; Jensen M Production of the Auger emitter 119Sb for targeted radionuclide therapy using a small PET-cyclotron. Appl. Radiat. Isot, 2009, 67(1), 34–38. 10.1016/j.apradiso.2008.09.003 [PubMed: 18990581]

[80]. Sadeghi M; Rovais MRA; Enferadi M; Sarabadani P Targetry and Radiochemistry for No-Carrier-Added Production of 117,118m,119,120m,122Sb. Nukleonika, 2011, 56(1), 9–15.

[81]. Gupta RK; Pramila GC; Srinivasa Raghavan R On the Decay of Te-119m and Te-119. Nucl. Phys, 1962, 32, 669–683. 10.1016/0029-5582(62)90369-3

[82]. Miller DA; Sun S; Yi JH Preparation of A118Te/118Sb Radionuclide Generator. J. Radioanal. Nucl. Chem. Artic, 1992, 160(2), 467–476. 10.1007/BF02037122

[83]. Miller DA; Sun S; Smithbauer S Separation of Radiotellurium from Proton-Irradiated Antimony Targets. Radiochim. Acta, 1992, 60(2–3), 69–74. 10.1524/ract.1993.60.23.69

[84]. Bennett KT; Bone SE; Akin AC; Birnbaum ER; Blake AV; Brugh M; Daly SR; Engle JW; Fassbender ME; Ferrier MG; Kozimor SA; Lilley LM; Martinez CA; Mocko V; Nortier FM; Stein BW; Thiemann SL; Vermeulen C Large-Scale Production of ^{119m}Te and ^{119}Sb for Radiopharmaceutical Applications. ACS Cent. Sci, 2019, 5(3), 494–505. 10.1021/acscentsci.8b00869 [PubMed: 30937377]

[85]. Downs D; Miller DA Radiochemical Separation of Antimony and Tellurium in Isotope Production and in Radionuclide Generators. J. Radioanal. Nucl. Chem, 2004, 262(1), 241–247. 10.1023/BJRNC.0000040881.44068.eb

[86]. Lagunas-Solar MC; Carvacho OF; Yang ST; Yano Y Cyclotron Production of PET Radionuclides: 118Sb (3.5 Min; B+ 75%; EC 25%) from High-Energy Protons on Natural Sb Targets. Int. J. Radiat. Appl. Instrumentation. Part, 1990, 41(6), 521–529. 10.1016/0883-2889(90)90033-D

[87]. Y Y; Lagunas-Solar MC Tellurium-118/Antimony-118 Generator. Proc. 36th Annu. Meet. Soc. Nucl. Med, 1989.

[88]. Macnevin WM; Lee IL The Separation of Mercury from Gold by Ion Exchange. Analyrica Chim. Acta, 1955, 12, 544–546. 10.1016/S0003-2670(00)87878-2

[89]. Gupta CB; Tandon SN Ion-Exchange Behavior Of Mercuryfll) In Mixed Solvents: Separation From Zinc(Ll), Cadmium(Ii), Gold(Lll), And Thallium(Lll). Sep. Sci, 1972, 7(5), 513–525. 10.1080/00372367208056051

[90]. Samczýnski Z Ion Exchange Behavior of Selected Elements on Chelex 100 Resin. Solvent Extr. Ion Exch., 2006, 24(5), 781–794. 10.1080/07366290600846174

[91]. Grote M; Kettrup A Analytica Chimica Acta; Elsevier Science Publishers B.V.: Amsterdam - Printed in The Netherlands, 1987.

[92]. Shah R; Devi S Dithizone-Anchored Poly(Vinylpyridine) as a Chelating Resin for the Preconcentration and Separation of Gold(III) from Platinum(IV), Copper(II) and Mercury(II). Analyst (Lond.), 1996, 121(6), 807–811. 10.1039/an9962100807

[93]. Moyers EM; Fritz JS Separation of Metal Ions Using a Hexylthioglycolate Resin.Anal. Chem, 1976, 48(8), 1117–1120. 10.1021/ac50002a013

[94]. Singh OV; Tandon SN Separation of Mercury(Ll) as Chloride from Zinc(Ll), Cadmium(Ll), Gold(Lll), and Thallium(Lll) by Extraction in High-Molecular-Weight Amines. Sep. Sci, 1975, 10(4), 359–370. 10.1080/00372367508058025

[95]. Nayak D; Lahiri S Production of Tracer Packet of Heavy and Toxic Elements. J. Radioanal. Nucl. Chem, 2002, 254(3), 619–623. 10.1023/A:1021670928426

[96]. Walther M; Lebeda O; Preusche S; Pietzsch HJ; Steinbach J Theranostic Mercury Part 1: A New Hg/Au Separation by a Resin Based Method. AIP Conf. Proc, 2017, 1845(5), 11–15. 10.1063/E4983554

[97]. White CE; Rose HJ Separation of Antimony by Solvent Extraction. Anal. Chem, 1953, 25(2), 351–353. 10.1021/ac60074a041

[98]. Hagebø E; Kjelberg A; Pappas AC Radiochemical Studies of Isotopes of Antimony and Tin in the Mass Region 127-130. J. Inorg. Nucl. Chem, 1962, 24(2), 117–131. 10.1016/S0022-1902(62)90084-2

[99]. Bock R; Hoppe T Über Die Trennung Anorganischer Stoffgemische Durch Verteilung. Anal. Chim. Acta, 1957, 16, 406–415. 10.1016/S0003-2670(00)89956-0

[100]. Vibhute RG; Khopkar SM Solvent extraction of antimony(III) with 18-crown-6 from iodide media. Talanta, 1989, 36(9), 957–959. 10.1016/0039-9140(89)80038-4 [PubMed: 18964841]

[101]. Sarkar SG; Dhadke PM Solvent Extraction Separation of Antimony (III) and Bismuth (III) with Bis(2,4,4-Trimethylpentyl) Monothiophosphinic Acid (Cyanex 302). Separ. Purif. Tech, 1999, 15(2), 131–138. 10.1016/S1383-5866(98)00088-4

[102]. Abecasis SM Fast Separation of Antimony from Irradiated Enriched Tellurium. Radiochim. Acta, 1963, 2(2), 103–104. 10.1524/ract.1963.2.2.103

[103]. Menon MP; Aras NK; Irvine JW Radiochemical Separation of Tin and Antimony by an Initial Phosphate Precipitation Step. J. Inorg. Nucl. Chem, 1965, 27(4), 767–771. 10.1016/0022-1902(65)80436-5

[104]. Kraus KA; Michelson DC; Nelson F Adsorption of Negatively Charged Complexes by Cation Exchangers. J. Am. Chem. Soc, 1959, 81(13), 3204–3207. 10.1021/ja01522a011

[105]. Minami E; Honda M; Sasaki Y Ion-Exchange Separation of Fission Products. Bull. Chem. Soc. Jpn, 1958, 31(3), 372–377. 10.1246/bcsj.31.372

[106]. Smith GW; Reynolds SA Anion Exchange Separation of Tin, Antimony and Tellurium. Analyrica Chim. Acta, 1955, 12, 151–153. 10.1016/S0003-2670(00)87822-8

[107]. Dawson J; Magee RJ The Anion-Exchange Separation of Tin and Antimony. Mikrochim. Acta, 1958, 46(3), 325–329. 10.1007/BF01216027

[108]. Maruyama Y; Yamaashi Y A Simple Method for the Separation of 125Sb from Neutron-Irradiated Tin. Int. J. Radiat. Appl. Instrumentation, 1988, 39(10), 1079–1080. 10.1016/0883-2889(88)90144-X

[109]. Baluev AV; Mityakhina VS; Krasnikov LV; Galkin BY; Beznosyuk VI Sb from Neutron-Irradiated Sn. Radiochemistry, 2003, 45(6), 616–619. 10.1023/B:RACH.0000015763.24494.ff

[110]. Cheremisina OV; Ponomareva MA; Sagdiev VN Sorption Recovery of Gallium and Aluminum from Alkaline Solutions on an AN-31 Anion Exchanger. Russ. J. Non-Ferrous Met, 2017, 58(4), 365–372. 10.3103/S1067821217040046

[111]. Takács S; Takács MP; Hermanne A; Tárkányi F; Adam Rebeles R Cross Sections of Proton Induced Reactions on NatSb. Nucl. Instruments Methods Phys. Res. Sect. B Beam Interact, with Mater. Atoms, 2013, 297, 44–57. 10.1016/j.nimb.2012.12.010

[112]. Mosby MA; Birnbaum ER; Nortier FM; Engle JW Cross Sections for Proton-Induced Reactions Onnat Sb up to 68 MeV. Nucl. Instruments Methods Phys. Res. Sect. B Beam Interact, with Mater. Atoms, 2017, ••• 10.1016/j.nimb.2017.08.038

[113]. Guin R; Das SK; Saha SK The Anion Exchange Behavior of Te and Sb. J. Radioanal. Nucl. Chem, 1998, 230(1–2), 269–272. 10.1007/BF02387477

[114]. Kim HN; Ren WX; Kim JS; Yoon J Fluorescent and colorimetric sensors for detection of lead, cadmium, and mercury ions. Chem. Soc. Rev, 2012, 41(8), 3210–3244. 10.1039/ClCS15245A [PubMed: 22184584]

[115]. Leiva-Presa A; Capdevila M; Gonzàlez-Duarte P Mercury(II) binding to metallothioneins. Variables governing the formation and structural features of the mammalian Hg-MT species. Eur. J. Biochem, 2004, 271(23-24), 4872–4880. 10.1111/j.1432-1033.2004.04456.x [PubMed: 15606775]

[116]. Wright JG; Natan MJ; Macdonnell FM; Ralston DM; Hallorant TVO Mercury(I1)-Thiolate Chemistry and the Mechanism of the Heavy Metal Biosensor MerR JEFFREY. Prog. Inorg. Chem. Bioinorg. Chem, 1990, 38, 325–412.

[117]. Utschig LM; Bryson JW; O'Halloran TV Mercury-199 NMR of the Metal Receptor Site in MerR and Its Protein-DNA Complex. Science (80-.), 1995, 268(5209), 380–385.

[118]. Ju H; Leech D Electrochemical Study of a Metallothionein Modified Gold Disk Electrode and Its Action on Hg2+ Cations. J. Electroanal. Chem. (Lausanne Switz.), 2000, 484(2), 150–156. 10.1016/S0022-0728(00)00071-1

[119]. Patrick L Mercury toxicity and antioxidants: Part 1: role of glutathione and alpha-lipoic acid in the treatment of mercury toxicity. Altern. Med. Rev, 2002, 7(6), 456–471. [PubMed: 12495372]

[120]. Kromidas L; Trombetta LD; Jamall IS The protective effects of glutathione against methylmercury cytotoxicity. Toxicol. Lett, 1990, 51(1), 67–80. 10.1016/0378-4274(90)90226-C [PubMed: 2315960]

[121]. Sen CK Nutritional Biochemistry of Cellular Glutathione. J. Nutr. Biochem, 1997, 8(12), 660–672. 10.1016/S0955-2863(97)00113-7

[122]. Oram PD; Fang X; Fernando Q; Letkeman P; Letkeman D The formation of constants of mercury(II)--glutathione complexes. Chem. Res. Toxicol, 1996, 9(4), 709–712. 10.1021/tx9501896 [PubMed: 8831814]

[123]. Stricks W; Kolthoff IM Reactions between Mercuric Mercury and Cysteine and Glutathione. Apparent Dissociation Constants, Heats and Entropies of Formation of Various Forms of Mercuric Mercapto-Cysteine and -Glutathione. J. Am. Chem. Soc, 1953, 75(22), 5673–5681. 10.1021/ja01118a060

[124]. Bebout DC Mercury: Inorganic & Coordination Chemistry-Based in Part on the Article Mercury: Inorganic & Coordination Chemistry by Gregory J. Grant Which Appeared in the Encyclopedia of Inorganic Chemistry, First Edition; , 2011.

[125]. Pearson RG; Songstad J Application of the Principle of Hard and Soft Acids and Bases to Organic Chemistry. J. Am. Chem. Soc, 1967, 89(8), 1827–1836. 10.1021/ja00984a014

[126]. Pearson RG Hard and Soft Acids and Bases. HSAB, Part 1: Fundamentals Principles. J. Chem. Educ, 1986, 45(12), 581–587.

[127]. Ho ML; Chen KY; Lee GH; Chen YC; Wang CC; Lee JF; Chung WC; Chou PT Mercury(II) recognition and fluorescence imaging *in vitro* through a 3D-complexation structure. Inorg. Chem, 2009, 48(21), 10304–10311. 10.1021/ic901613s [PubMed: 19852521]

[128]. Park S; Lee SY; Jo M; Lee JY; Lee SS Molecular Botanical Garden: Assembly of Supramolecular Silver(I) and Mercury(II) Complexes of NS2-Donor Macrocycles with Flower-, Leaf- and Tree-Shaped Structures. CrystEngComm, 2009, 11(1), 43–46. 10.1039/B814051K

[129]. Riccardi D; Guo HB; Parks JM; Gu B; Summers AO; Miller SM; Liang L; Smith JC Why Mercury Prefers Soft Ligands. J. Phys. Chem. Lett, 2013, 4(14), 2317–2322. 10.1021/jz401075b

[130]. Cooper SR Crown Thioether Chemistry. Acc. Chem. Res, 1988, 21(4), 141–146. 10.1021/ar00148a002

[131]. Bond AM; Colton R; Ebner J Multinuclear Magnetic Resonance (31P, 77Se, 199Hg) and Electrochemical Studies of Nonlabile Mercury(II) Complexes with Group 15/Group 16 Donor Ligands. Inorg. Chem, 1988, 27(10), 1697–1702. 10.1021/ic00283a008

[132]. Levason W; Orchard SD; Reid G Recent Developments in the Chemistry of Selenoethers and Telluroethers. Coord. Chem. Rev, 2002, 225(1–2), 159–199. 10.1016/S0010-8545(01)00412-X

[133]. Singh AK; Thomas S; Khandelwal BL Preparative and Spectral Investgation on Ortho-Tellurated Phenenols and Their Mercury(II), Palladium(II) and Platinum(II) Phenoxides and Chelated through Tellurium. Polyhedron, 1991, 10(23/24), 2693–2697. 10.1016/S0277-5387(00)86169-0

[134]. Atwood DA; Bebout DC; Berry SM Recent Development in Mercury Science;, 2006.

[135]. Bebout DC; Bush JF II; Crahan KK; Kastner ME; Parrish DA Correlation of a Solution-State Conformational Change between Mercuric Chloride Complexes of Tris[(2-(6-methylpyridyl))methyl]amine with X-ray Crystallographic Structures. Inorg. Chem, 1998, 37(18), 4641–4646. 10.1021/ic980296y [PubMed: 11670615]

[136]. Bebout DC; Stokes SW; Butcher RJ Comparison of Heteronuclear Coupling Constants for Isostructural Nitrogen Coordination Compounds of (111/113)Cd and (199)Hg. Inorg. Chem, 1999, 38(6), 1126–1133. 10.1021/ic980825y [PubMed: 11670894]

[137]. Bebout DC; Bush JF; Shumann EM; Viehweg JA; Kastner ME; Parrish DA; Baldwin SM Caging the Mercurous Ion: A Tetradentate Tripodal Nitrogen Ligand Enhances Stability and J(1H199Hg). J. Chem. Crystallogr, 2003, 33(5–6), 457–463. 10.1023/A:1024246501525

[138]. Bebout DC; Bush JF II; Crahan KK; Bowers EV; Butcher RJ Sterically demanding multidentate ligand tris[(2-(6-methylpyridyl))methyl] amine slows exchange and enhances solution state

ligand proton NMR coupling to (199)Hg(II). Inorg. Chem, 2002, 41(9), 2529–2536. 10.1021/ic011209w [PubMed: 11978122]

[139]. Morsali A; Masoomi MY Structures and Properties of Mercury(II) Coordination Polymers. Coord. Chem. Rev, 2009, 253(13–14), 1882–1905. 10.1016/j.ccr.2009.02.018

[140]. Atkins P; Overton T; Rourke J; Weller M; Armstrong F; Hagerman M Inorganic Chemistry, Armstmg J; Dann S; Egdell R; Creen J; Jones M; Deeth R, Eds.; W.H. Freeman and Company: New York, 2008.

[141]. Holloway CE; Melnik M Mercury Coordination Compounds: Classification and Analysis of Crystallographical and Structural Data. Main Group Met. Chem, 1994, 17(11–12), 799–885. 10.1515/MGMC.1994.17.11-12.799

[142]. Schlager O; Wieghardt K; Grondey H; Rufmska A; Nuber B The Hexadentate Ligand 1.4.7-Tris (o-Aminobenzyl)-l,4,7-Triazacyclononane and Its Complexes with Zinc(II), Cadmium(II), and Mercury(II) in Solution and in the Solid State. Inorg. Chem, 1995, 34(26), 6440–6448. 10.1021/ic00130a008

[143]. Bishop DB; McCool GD; Nelson AJ; Reynolds JG; Baumann TF; Fox GA; DeWitt JG; Andrews JC X-Ray Absorption Spectroscopy of Thiacrown Compounds Used in the Remediation of Mercury Contaminated Water. Microchem. J, 2002, 71(2–3), 247–254. 10.1016/S0026-265X(02)00016-4

[144]. Tsuchiya T; Shimizu T; Hirabayashi K; Kamigata N Formation and structures of mercury complexes of 18-membered unsaturated and saturated thiacrown ethers. J. Org. Chem, 2003, 68(9), 3480–3485. 10.1021/jo020668r [PubMed: 12713349]

[145]. Helm ML; Helton GP; Vanderveer DG; Grant GJ Mercury-199 NMR studies of thiacrown and related macrocyclic complexes: the crystal structures of [Hg(18S6)](PF6)2 and [Hg(9N3)2] (C104)2. Inorg. Chem, 2005, 44(16), 5696–5705. 10.1021/ic050500z [PubMed: 16060620]

[146]. Chen S; Kim E; Shuler ML; Wilson DB Hg2+ removal by genetically engineered Escherichia coli in a hollow fiber bioreactor. Biotechnol. Prog, 1998, 14(5), 667–671. 10.1021/bp980072i [PubMed: 9758654]

[147]. Blake AJ; Reid G; Schroder M MERCURY MACROCYCLIC COMPLEXES : THE SYNTHESIS OF [Hg([18]A-neN2S4)]2= AND [Hg(Me,[18]AneN,S4)]2+. THE SINGLE CRYSTAL X-RAY STRUCTURE OF [Hg([18]AneN2S2)](PF6) 4/3H2O ALEXANDER. Polyhedron, 1990, 9(24), 2931–2935. 10.1016/S0277-5387(00)84203-5

[148]. Bach RD; Vardhan HBA 199Hg NMR Study of the Complexation of Methylmercury with Thia-Crown Ethers. The Absence of a Macrocyclic Ligand Effect. J. Org. Chem, 1986, 51(9), 1609–1610. 10.1021/jo00359a046

[149]. Helm ML; Vanderveer DG; Grant GJ Mercury Complexes with Thiacrowns: The Crystal Structure of Bis(1,4,7-Trithiacyclodecane)Mercury(II) Hexafluorophosphate. J. Chem. Crystallogr, 2003, 33(8), 625–630. 10.1023/A:1024954028516

[150]. Blower PJ; Smith RJ; Jolley C Thiamacrocyclic Bifunctional Chelators for Labelling Antibodies with Chemically "soft" Radiometals. Nucl. Med. Commun, 1992, 13(4), 231. 10.1097/00006231-199204000-00085

[151]. Nolan EM; Lippard SJAA "turn-on" fluorescent sensor for the selective detection of mercuric ion in aqueous media. J. Am. Chem. Soc, 2003, 125(47), 14270–14271. 10.1021/ja037995g [PubMed: 14624563]

[152]. Mori A; Kubo K; Takeshita H Synthesis and Metallophilic Properties of Troponoid Thiocrown Ethers. Coord. Chem. Rev, 1996, 148, 71–96. 10.1016/0010-8545(95)01174-9

[153]. Baumann TF; Reynolds JG; Fox GA Polymer Pendant Crown Thioethers: Synthesis and HgII Extraction Studies of a Novel Thiacrown Polymer. Chem. Commun. (Camb.), 1998, (16), 1637–1638. 10.1039/a803383h

[154]. Atilgan S; Kutuk I; Ozdemir T A near IR Di-Styryl BODIPY-Based Ratiometric Fluorescent Chemosensor for Hg(II). Tetrahedron Lett., 2010, 51(6), 892–894. 10.1016/j.tetlet.2009.12.025

[155]. Shi W; Ma H Spectroscopic probes with changeable π-conjugated systems. Chem. Commun. (Camb.), 2012, 48(70), 8732–8744. 10.1039/c2cc33366j [PubMed: 22790022]

[156]. Huang J; Xu Y; Qian X A Rhodamine-Based Hg 2 + Sensor with High Selectivity and Sensitivity in Aqueous Solution : A NS 2 -Containing Receptor S CHEME 1. Representative

Mechanism of the Chemosensor Based on the RhB A Rhodamine-Based Sensor 1 Was Designed and Synthesized NS 2 W. J. Org. Chem, 2009, 74(c), 5039–5042.

[157]. Kwon SK; Kim HN; Rho JH; Swamy KMK; Shanthakumar SM; Yoon J Rhodamine Derivative Bearing Histidine Binding Site as a Fluorescent Chemosensor for Hg2+. Bull. Korean Chem. Soc, 2009, 30(3), 719–721. 10.5012/bkcs.2009.30.3.719

[158]. Chen X; Baek KH; Kim Y; Kim SJ; Shin I; Yoon J A Selenolactone-Based Fluorescent Chemodosimeter to Monitor Mecury/Methylmercury Species in Vitro and in Vivo. Tetrahedron, 2010, 66(23), 4016–4021. 10.1016/j.tet.2010.04.042

[159]. Bazzicalupi C; Caltagirone C; Cao Z; Chen Q; Di Natale C; Garau A; Lippolis V; Lvova L; Liu H; Lundström I; Mostallino MC; Nieddu M; Paolesse R; Prodi L; Sgarzi M; Zaccheroni N Multimodal use of new coumarin-based fluorescent chemosensors: towards highly selective optical sensors for Hg(2+) probing. Chemistry, 2013, 19(43), 14639–14653. 10.1002/chem.201302090 [PubMed: 24027223]

[160]. Han ZX; Luo HY; Zhang XB; Kong RM; Shen GL; Yu RQ A ratiometric chemosensor for fluorescent determination of Hg(2+) based on a new porphyrin-quinoline dyad. Spectrochim. Acta A Mol. Biomol. Spectrosc, 2009, 72(5), 1084–1088. 10.1016/j.saa.2009.01.003 [PubMed: 19233718]

[161]. Zheng QY; Chen CF; Huang ZT A Facile Method for Synthesis of Calix[4]Crowns Containing Nitrogen and Sulfur Atoms. J. Chem. Res, 1999, 3, 212–213.

[162]. Fang CL; Zhou J; Liu XJ; Cao ZH; Shangguan DH Mercury(II)-mediated formation of imide-Hg-imide complexes. Dalton Trans, 2011, 40(4), 899–903. 10.1039/C0DT01118E [PubMed: 21152558]

[163]. Chen T; Zhu W; Xu Y; Zhang S; Zhang X; Qian X A thioether-rich crown-based highly selective fluorescent sensor for Hg(2+) and Ag(+) in aqueous solution. Dalton Trans, 2010, 39(5), 1316–1320. 10.1039/B908969A [PubMed: 20104358]

[164]. Vaswani KG; Keränen MD Detection of aqueous mercuric ion with a structurally simple 8-hydroxyquinoline derived ON-OFF fluorosensor. Inorg. Chem, 2009, 48(13), 5797–5800. 10.1021/ic9004517 [PubMed: 19496544]

[165]. Sadhu KK; Sen S; Bharadwaj PK Cryptand derived fluorescence signaling systems for sensing Hg(II) ion: A comparative study. Dalton Trans, 2011, 40(3), 726–734. 10.1039/C0DT01005G [PubMed: 21120252]

[166]. Yang Y; Jiang J; Shen G; Yu R An optical sensor for mercury ion based on the fluorescence quenching of tetra(p-dimethylaminophenyl)porphyrin. Anal. Chim. Acta, 2009, 636(1), 83–88. 10.1016/j.aca.2009.01.038 [PubMed: 19231360]

[167]. Tan ZQ; Liu JF Visual test of subparts per billion-level mercuric ion with a gold nanoparticle probe after preconcentration by hollow fiber supported liquid membrane. Anal. Chem, 2010, 82(10), 4222–4228. 10.1021/acl00541s [PubMed: 20405900]

[168]. Lo SI; Chen PC; Huang CC; Chang HT Gold nanoparticle-aluminum oxide adsorbent for efficient removal of mercury species from natural waters. Environ. Sci. Technol, 2012, 46(5), 2724–2730. 10.1021/es203678v [PubMed: 22309110]

[169]. Wang Y; Yang F; Yang X Colorimetric biosensing of mercury(II) ion using unmodified gold nanoparticle probes and thrombin-binding aptamer. Biosens. Bioelectron, 2010, 25(8), 1994–1998. 10.1016/j.bios.2010.01.014 [PubMed: 20138750]

[170]. Pradeep T Anshup. Noble Metal Nanoparticles for Water Purification: A Critical Review. Thin Solid Films, 2009, 517(24), 6441–6478. 10.1016/j.tsf.2009.03.195

[171]. Huang CC; Yang Z; Lee KH; Chang HT Synthesis of highly fluorescent gold nanoparticles for sensing mercury(II). Angew. Chem. Int. Ed. Engl, 2007, 46(36), 6824–6828. 10.1002/anie.200700803 [PubMed: 17674391]

[172]. Lisha K.P. Anshup; Pradeep T Towards a Practical Solution for Removing Inorganic Mercury from Drinking Water Using Gold Nanoparticles. Gold Bull, 2009, 42(2), 144–152. 10.1007/BF03214924

[173]. Coates RL; Jones MM Stability Constants of the BAL Complexes., 1977, 39, 677–678.

[174]. Casas JS; Jones MM Mercury(II) Complexes with Sulfhydryl Containing Chelating Agents: Stability Constant Inconsistencies and Their Resolution. J. Inorg. Nucl. Chem, 1980, 42(1), 99–102. 10.1016/0022-1902(80)80052-2

[175]. Bjørklund G; Crisponi G; Nurchi VM; Cappai R; Buha Djordjevic A; Aaseth J A Review on Coordination Properties of Thiol-Containing Chelating Agents Towards Mercury, Cadmium, and Lead. Molecules, 2019, 24(18), 1–32. 10.3390/molecules24183247

[176]. Aaseth J; Ajsuvakova OP; Skalny AV; Skalnaya MG; Tinkov AA Chelator Combination as Therapeutic Strategy in Mercury and Lead Poisonings. Coord. Chem. Rev, 2018, 358, 1–12. 10.1016/j.ccr.2017.12.011

[177]. Fang X; Hua F; Fernando Q Comparison of rac- and meso-2,3-dimercaptosuccinic acids for chelation of mercury and cadmium using chemical speciation models. Chem. Res. Toxicol, 1996, 9(1), 284–290. 10.1021/tx950096o [PubMed: 8924605]

[178]. Basinger MA; Casas JS; Jones MM; Weaver AD; Weinstein NH Structural Requirements for Mercury(II) Antidotes. J. Inorg. Nucl. Chem, 1981, 43(6), 1419–1425. 10.1016/0022-1902(81)80058-9

[179]. Aposhian HV; Maiorino RM; Gonzalez-Ramirez D; Zuniga-Charles M; Xu Z; Hurlbut KM; Junco-Munoz P; Dart RC; Aposhian MM Mobilization of heavy metals by newer, therapeutically useful chelating agents. Toxicology, 1995, 97(1-3), 23–38. 10.1016/0300-483X(95)02965-B [PubMed: 7716789]

[180]. Greif RL; Sullivan WJ; Jacobs GS; Pitts RF Distribution of radiomercury administered as labelled chlormerodrin (neohydrin) in the kidneys of rats and dogs. J. Clin. Invest, 1956, 35(1), 38–43. 10.1172/JCI103250 [PubMed: 13278399]

[181]. Ter-pogossian MM; Ph D Comparative Study of Mercury-197 Chlormerodrin And Mercury-203 Chlormerodrin For Brain Scanning. J. Nucl. Med, 1966, 7(1), 50–59.

[182]. Wang Y; Westerman MP; Heinle EW Spleen-function study with 1-mercuri-2-hydroxypropane labeled with mercury 197. JAMA, 1965, 194(11), 1254–1256. 10.1001/jama.1965.03090240088034 [PubMed: 5897756]

[183]. Drozdovitch V; Brill AB; Callahan RJ Use of Radiopharmaceuticals in Diagnostic Nuclear Medicine in the United States: 1960-2010, 2016, 108

[184]. Reba RC; McAfee JG; Wagner HN, Jr Radiomercury-Labelled Chlormerodrin for in Vivo Uptake Studies and Scintillation Scannin Gof Unilateral Renal Lesions Associated with Hypertension. Medicine (Baltimore), 1963, 42(2), 269–296. 10.1097/00005792-196307000-00002 [PubMed: 14046753]

[185]. Saha GB; Schell ET; Farrer PA Labeling human lymphocytes with mercury-197. J. Nucl. Med, 1977, 18(1), 70–73. [PubMed: 830833]

[186]. Wardell JL Arsenic, Antimony, and Bismuth, 2011, pp. 157–165.

[187]. Fischer RC Antimony: Inorganic Chemistry. Encycl. Inorg. Bioinorg. Chem, 2016, 3, 1–13.

[188]. Laintz KE; Shieh GM; Wai CM Simultaneous determination of arsenic and antimony species in environmental samples using bis(trifluoroethyl)dithiocarbamate chelation and supercritical fluid chromatography. J. Chromatogr. Sci, 1992, 30(4), 120–123. 10.1093/chromsci/30.4.120 [PubMed: 1400861]

[189]. Maroulis G Atoms, Molecules and Clusters in Electric Fields'; , 2006.

[190]. Maroulis G Cluster Size Effect on the Electric Polarizability and Hyperpolarizability in Small Antimony Clusters Sbn, n = 1, 2 and 4. Chem. Rhys. Lett, 2007, 444(1–3), 44–47. 10.1016/j.cplett.2007.07.015

[191]. Jones C Recent Developments in Low Coordination Organo-Antimony and Bismuth Chemistry. Coord. Chem. Rev, 2001, 215(1), 151–169. 10.1016/S0010-8545(00)00405-7

[192]. Breunig HJ; Rat CI Catenated Compounds - Group 15 (As, Sb, Bi). Comprehensive Inorganic Chemistry II from elements to applications, 2013, 15, 151–178.

[193]. Boelaert M; Sundar S *Manson's Tropical Diseases*; Manson's Tropical Diseases, 2014, pp. 631–651. 10.1016/B978-0-7020-5101-2.00048-0

[194]. Croft SL; Sundar S; Fairlamb AH Drug resistance in leishmaniasis. Clin. Microbiol. Rev, 2006, 19(1), 111–126. 10.1128/CMR.19.1.111-126.2006 [PubMed: 16418526]

[195]. Tiekink ERT Antimony and bismuth compounds in oncology. Crit. Rev. Oncol. Hematol, 2002, 42(3), 217–224. 10.1016/S1040-8428(01)00217-7 [PubMed: 12050016]

[196]. Hu S-Z; Fu Y-M; Xu B; Tang W-D; Yu W-J Studies of the Antitumor Antimony(III) Triaminocarboxylic Complexonates. Crystal Structures of NH4[Sb(Hdtpa)]*H2O and Na[Sb(Hdtpa)]*4.5H2O (Dtpa=diethylenetriaminepentaacetic Acid). Main Group Met. Chem, 1997, 20(3), 169–180. 10.1515/MGMC.1997.20.3.169

[197]. Hadjikakou SK; Antoniadis CD; Hadjiliadis N; Kubicki M ; Binolis J; Karkabounas S; Charalabopoulos K Synthesis and Characterization of New Water Stable Antimony(III) Complex with Pyrimidine-2-Thione and in Vitro Biological Study. Inorganica Chim. Acta, 2005.

[198]. Blaurock-Busch E Comparison of Chelating Agents DMPS, DMSA and EDTA for the Diagnosis and Treatment of Chronic Metal Exposure. Br. J. Med. Med. Res, 2014, 4(9), 1821–1835. 10.9734/BJMMR/2014/6875

[199]. Garje SS; Jain VK Chemistry of Arsenic, Antimony and Bismuth Compounds Derived from Xanthate, Dithiocarbamate and Phosphorus Based Ligands. Coord. Chem. Rev, 2003, 236(1–2), 35–56. 10.1016/S0010-8545(02)00159-5

[200]. Ozturk II Novel Antimony(III) Halide Complexes with Some n-Alkyl Thioureas: Synthesis, Characterization and Study of Their Effect upon the Catalytic Oxidation of Linoleic Acid to Hydroperoxylinoleic Acid by Lipoxygenase. JOTCSA, 2017, 44(41), 81–9881. 10.18596/jotcsa.31798

[201]. Besold J; Kumar N; Scheinost AC; Lezama Pacheco J; Fendorf S; Planer-Friedrich B Antimonite Complexation with Thiol and Carboxyl/Phenol Groups of Peat Organic Matter. Environ. Sci. Technol, 2019, 53(9), 5005–5015. 10.1021/acs.est.9b00495 [PubMed: 30973221]

[202]. Ferraz KSO; Silva NF; da Silva JG; de Miranda LF; Romeiro CFD; Souza-Fagundes EM; Mendes IC; Beraldo H Investigation on the pharmacological profile of 2,6-diacetylpyridine bis(benzoylhydrazone) derivatives and their antimony(III) and bismuth(III) complexes. Eur. J. Med. Chem, 2012, 53, 98–106. 10.1016/j.ejmech.2012.03.040 [PubMed: 22520151]

[203]. DeGraffenreid AJ; Feng Y; Barnes CL; Ketring AR; Cutler CS; Jurisson SS Trithiols and their arsenic compounds for potential use in diagnostic and therapeutic radiopharmaceuticals. Nucl. Med. Biol, 2016, 43(5), 288–295. 10.1016/j.nucmedbio.2016.01.005 [PubMed: 27150031]

[204]. Feng Y; Jurisson SS Trithiol Compounds—Tricky but Valuable: The Design and Synthesis of Ligands for Stabilizing Radioarsenic for Radiopharmaceutical Development. Strateg. Tactics Org. Synth, 2019, 14, 207–224. 10.1016/B978-0-12-814805-l.00008-9

[205]. Feng Y; DeGraffenreid AJ; Phipps MD; Rold TL; Okoye NC; Gallazzi FA; Barnes CL; Cutler CS; Ketring AR; Hoffman TJ; Jurisson SS A trithiol bifunctional chelate for ^{72,77}As: A matched pair theranostic complex with high *in vivo* stability. Nucl. Med. Biol, 2018, 61, 1–10. 10.1016/j.nucmedbio.2018.03.001 [PubMed: 29571038]

[206]. Clarkson TW Chapter 61 - Inorganic and Organometal Pesticides. *Handbook of Pesticide Toxicology*;, 2001, pp. 1357–1428.

[207]. Thakur ML; Clark JC; Silvester DJ The production of 177-S-b-labelled potassium antimonyl tartrate for medical use. Int. J. Appl. Radiat. Isot, 1970, 21(1), 33–36. 10.1016/0020-708X(70)90033-5 [PubMed: 5415010]

[208]. Howell RW Radiation spectra for Auger-electron emitting radionuclides: report No. 2 of AAPM Nuclear Medicine Task Group No. 6. Med. Rhys, 1992, 19(6), 1371–1383. 10.1118/1.596927

[209]. Lovchikova GN; Salnikov OA; Simakov SP; Trufanov AM; Kotelnikova GV; Pilz V; Streil T Investigation of Mechanism of the Reactions 94-Zr(p,n) 94-Nb, 119-Sn(p,n) 119-Sb, 122-Sn(p,n) 122-Sb in the Proton Energy Region 6-9 MeV. Solviet J. Nucl. Rhys, 1980, 31, 3.

[210]. Johnson CH; Kernell RL (P,n) Cross Sections and the Strength Functions for 3- to 5.5-MeV Protons on In and on Sn Isotopes. Phys. Rev. Part C. Nucl. Phys, 1970, 2, 639.

[211]. Johnson CH; Bair JK; Jones CM; Penny SK; Smith DW Wave Size Resonances Observed by the (p,n) Reaction for 2.6- to 7-MeV Protons Incident on Isotopes of Sn. Phys. Rev. Part C. Nucl. Rhys, 1977, 15, 196.

[212]. Tárkányi F; Ditrói F; Hermanne A; Takács S; Király B; Baba M; Ignatyuk AV Experimental Study of the Excitation Functions of Deuteron Induced Reactions OnnatSn up to 40 MeV. Nucl.

Instruments Methods Phys. Res. Sect. B Beam Interact. with Mater. Atoms, 2011, 269(4), 405–416. 10.1016/j.nimb.2010.12.041

[213]. Hermanne A; Tárkányi F; Ditrói F; Takács S Extension of the Excitation Functions of Deuteron Induced Reactions on NatSn up to 50 MeV. Nucl. Instruments Methods Phys. Res. Sect. B Beam Interact. with Mater. Atoms, 2017, 391, 1–9. 10.1016/j.nimb.2016.11.005

[214]. Yi JH; Miller DA Cross Sections of NatSb(p,x) Reactions for 30-46 MeV Protons. Int. J. Radiat. Appl. Instrumentation. Part, 1992, 43(9), 1103–1106. 10.1016/0883-2889(92)90051-F

[215]. Elbinawi A; Al-Abyad M; Abd-Elmageed KE; Hassan KF; Ditroi F Proton Induced Nuclear Reactions on Natural Antimony up to 17 MeV. Radiochim. Acta, 2016, 104(4), 221–226. 10.1515/ract-2015-2483

[216]. Batij VG; Skakun EA; Rastrepin OA; Baskova KA; Makuni BM; Chugaj TV; Shavtvalov LJ Excitation Functions (p,n) and (a,Xn) Reactions with Formation of Te-119-m,g and Te-121-m,g Isomeric Pairs. Conf. 32 Conference on Nuclear Spectral Atomic Nuclear Structure, 1982, p. 134.

[217]. Takács S; Takács MP; Hermanne A; Tárkányi F; Adam Rebeles R Cross Sections of Deuteron-Induced Reactions on NatSb up to 50 MeV. Nucl. Instruments Methods Phys. Res. Sect. B Beam Interact. with Mater. Atoms, 2012, 278, 93–105. 10.1016/j.nimb.2012.02.007

[218]. Batij VG; Baskova KA; Kuz'menko VA; Makuni BM; Rastrepin OA; Skaku EA; Chugaj TV; Shavtvalov LJ Excitation Functions of Sn-116,117(a,Xn) Reactions in the Energy Range Under 30 MeV. Conf. 34 Conference on Nuclear Spectral Atomic Nuclear Structure, 1984, p. 355.

[219]. Filipescu D; Avrigeanu V; Glodariu T; Mihai C; Bucurescu D; Ivascu M; Cata-Danil I; Stroe L; Sima O; Cata-Danil G; Deleanu D; Ghita DG; Marginean N; Marginean R; Negret A; Pascu S; Sava T; Suliman G; Zamfir NV Cross Sections for Alpha-Particle Induced Reactions on 115,116Sn around the Coulomb Barrier. Phys. Rev. Part C. Nucl. Phys, 2011, 83, 64609.

[220]. Antropov AE; Khamid V; Smirnov AV; Kolozhvari AA; Gusev VP; Zarubin PP; Kordyukevich VO; Giruts VL Analysis of Excitation Function of Alpha-Particle Induced Reactions on 116,117,118,120,124 Sn at the Energies of 13-24.4 MeV. International Conference on Nuclear Spectroscopy and Nuclear Structure, 1992, p. 288.

[221]. Vystoskiy ON; Gaydaenko SA; Gonchar AV; Zaritskiy VS; Kadkin EP; Kondrat'ev SN; Lobach YN; Prokopenko VS; Saltykov LS; Sklyarenko VD; Stepanenko VA; Tokarevskiy VV Excitation Functions Sn-Natur(He3,X) Reaction with Formation Radionuclides at He-3 Ions Energy to 95 MeV. Conf. 43 Conference on Nuclear Spectoscopy and Nuclear Structure, 1993, p. 257.

[222]. Hinghofer-Szalkay H; Greenleaf JE Continuous monitoring of blood volume changes in humans. J Appl Physiol (1985), 1987, 63(3), 1003–1007. 10.1152/jappl.1987.63.3.1003 [PubMed: 3654450]
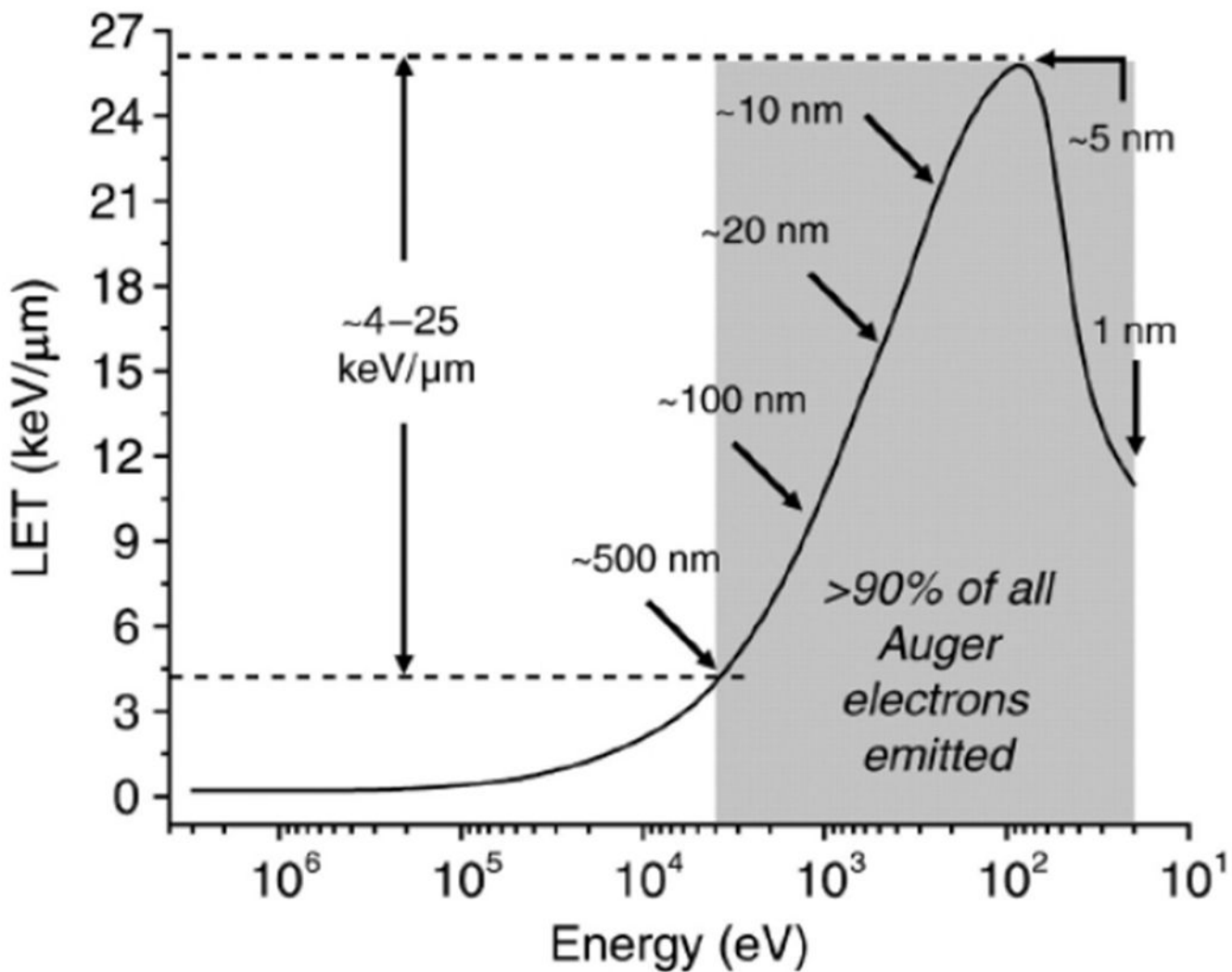
Fig. (1).
LET of electrons as function of their energy. Arrows indicate the range of electrons at
each specified energy. Image Modified and reproduced Kassis, A. I. Molecular and Cellular
Radiobiological Effects of Auger Emitting Radionuclides. Radiat. Prot. Dosimetry 2011,
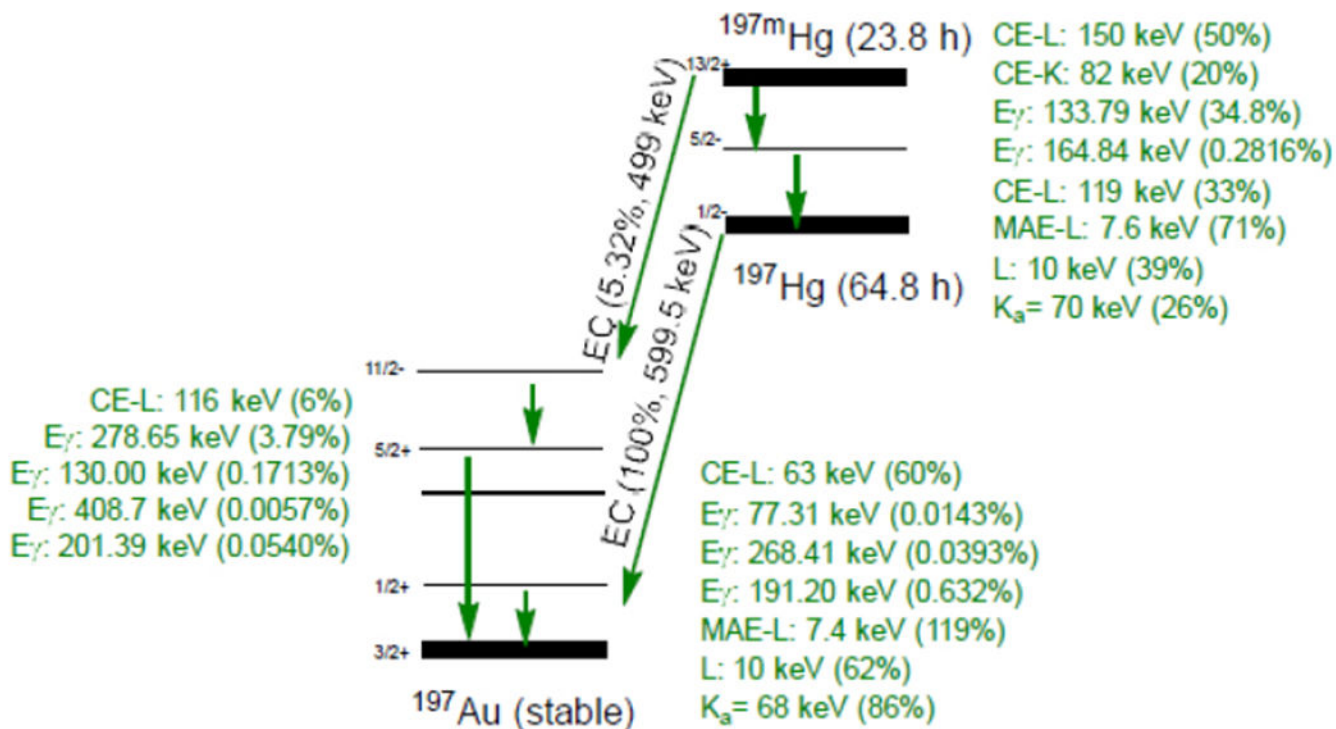143 (2—4), 241–247. by permission of Oxford University Press [19].

Fig. (2).
Decay scheme of $^{197m/g}$Hg depicting the useful photon emissions and MAE and CE emissions. [34–36]. (*A higher resolution / colour version of this figure is available in the electronic copy of the article*).
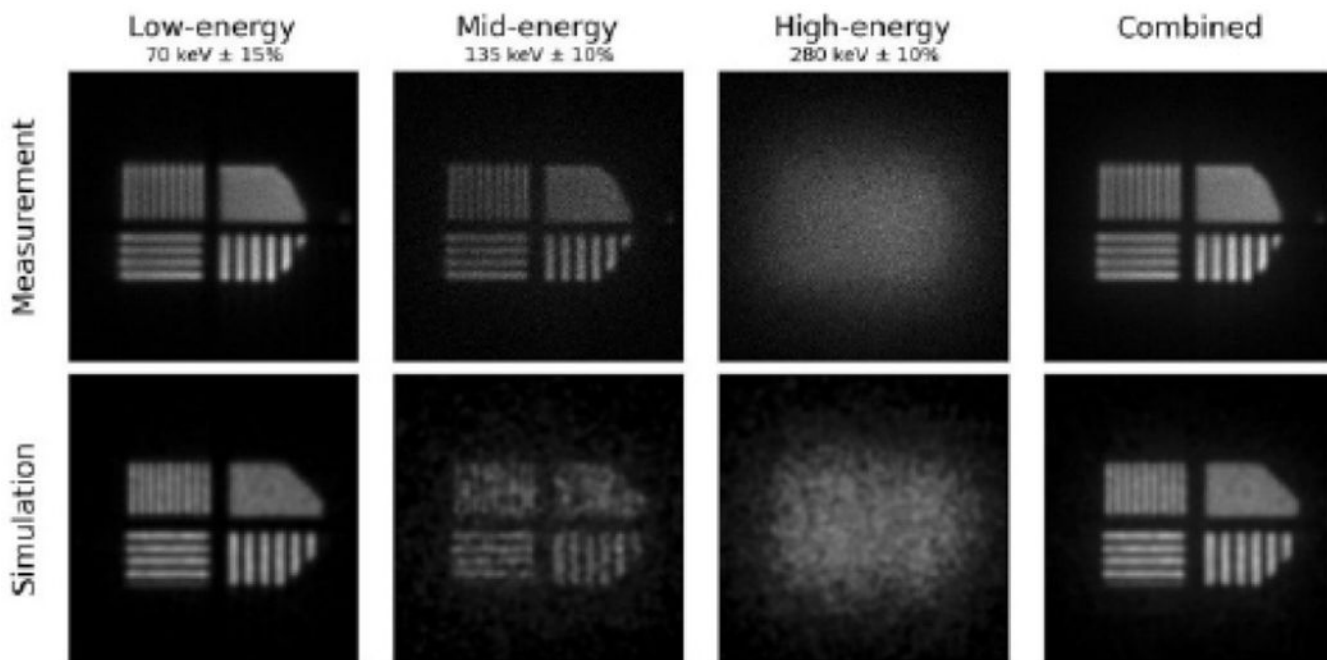
Fig. (3).

The phantom images of the measurements by the Philips BrightView SPECT camera and by Monte Carlo simulation. The planer decomposition of the three gamma ray energies produced in the decay of $^{197m/g}$Hg is shown as well as their combination. Image reporduce from [18]. (*A higher resolution / colour version of this figure is available in the electronic copy of the article*).
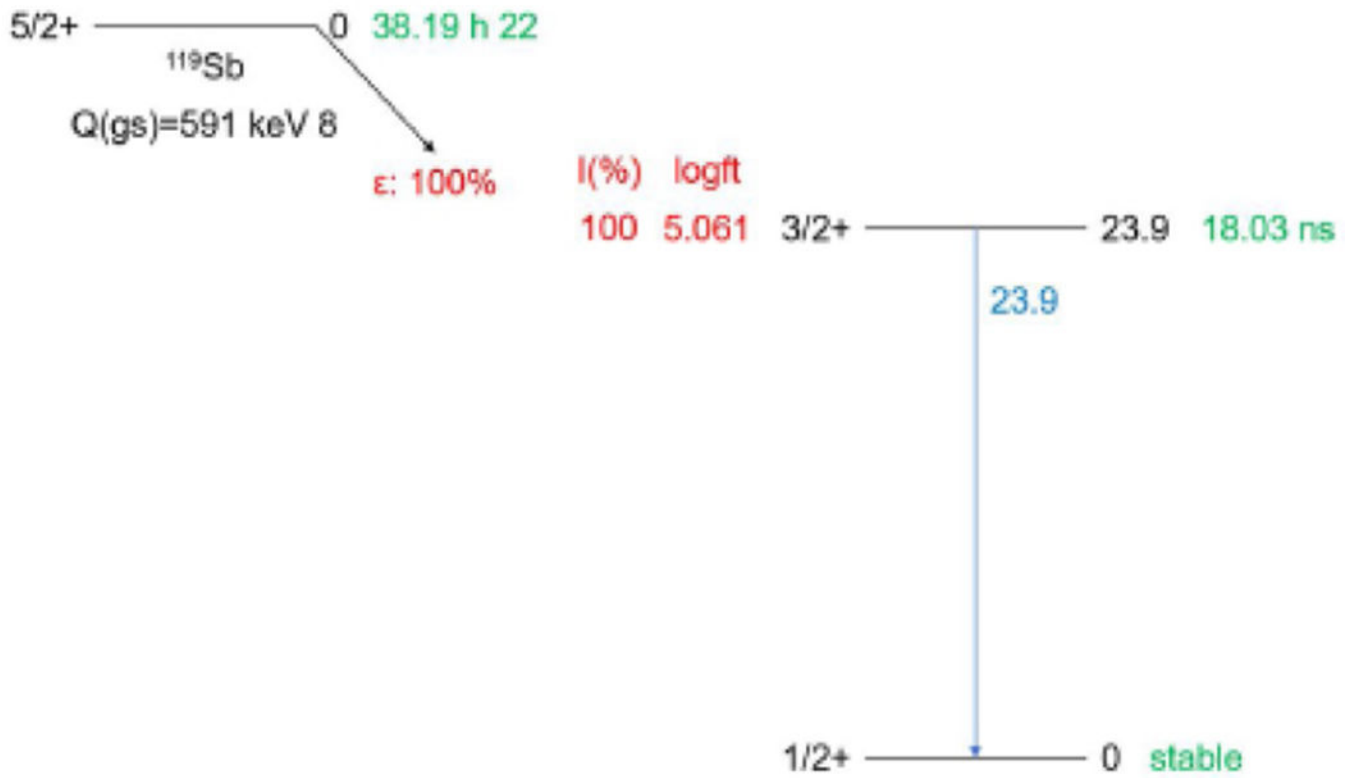
Fig. (4).
Decay scheme of [119]Sb [52]. (*A higher resolution / colour version of this figure is available in the electronic copy of the article*).
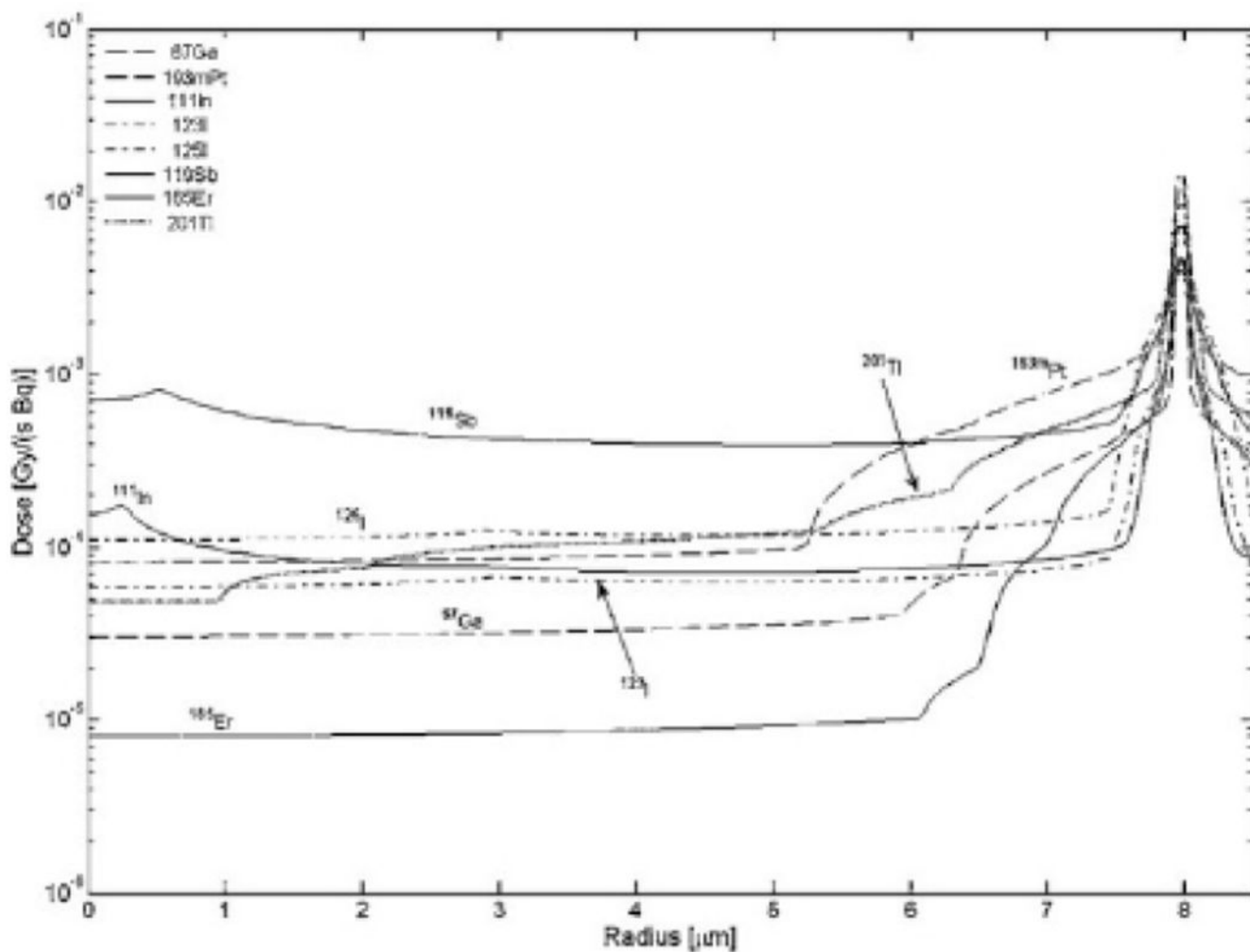
Fig. (5).
Dose deposited to various parts of a cell per cumulated decay as a function of radius for a uniform activity distribution on the cell surface, depicting [119]Sb providing the greatest dose to the nucleus from compared radionuclides. Figure taken from [55]. (*A higher resolution / colour version of this figure is available in the electronic copy of the article*).
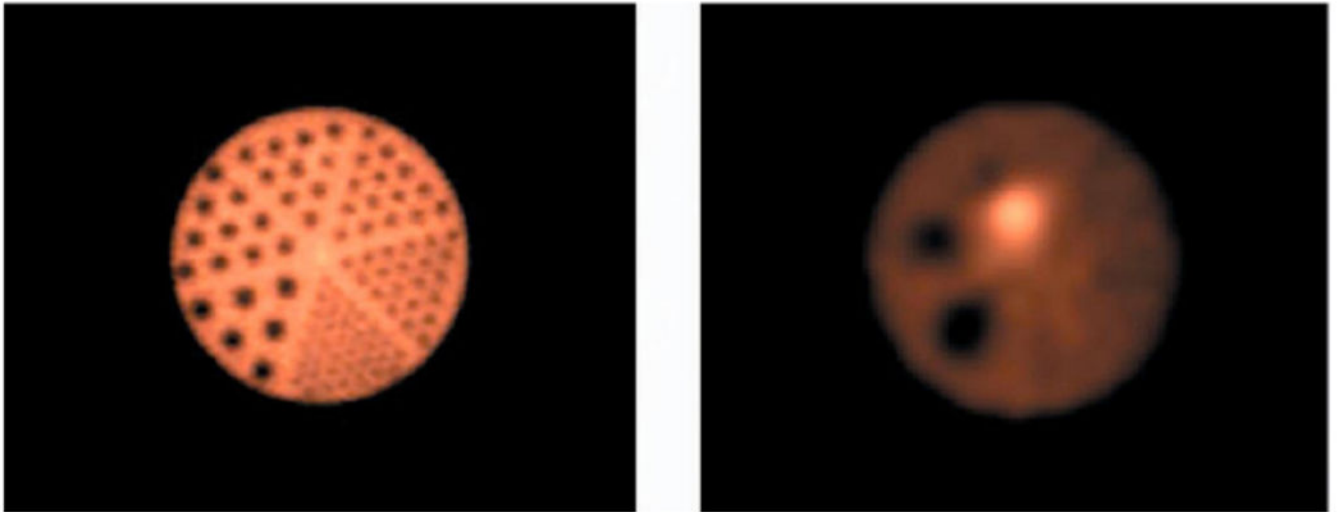
Fig. (6).
(Left) planar scintography image of ^{117}Sb homogenously distributed in Jazczak phantom with cold rod inserts. (right) SPECT image of ^{117}Sb uniform background, cold sphere inserts, and hot insert. Image reprinted from [55]. (*A higher resolution / colour version of this figure is available in the electronic copy of the article*).
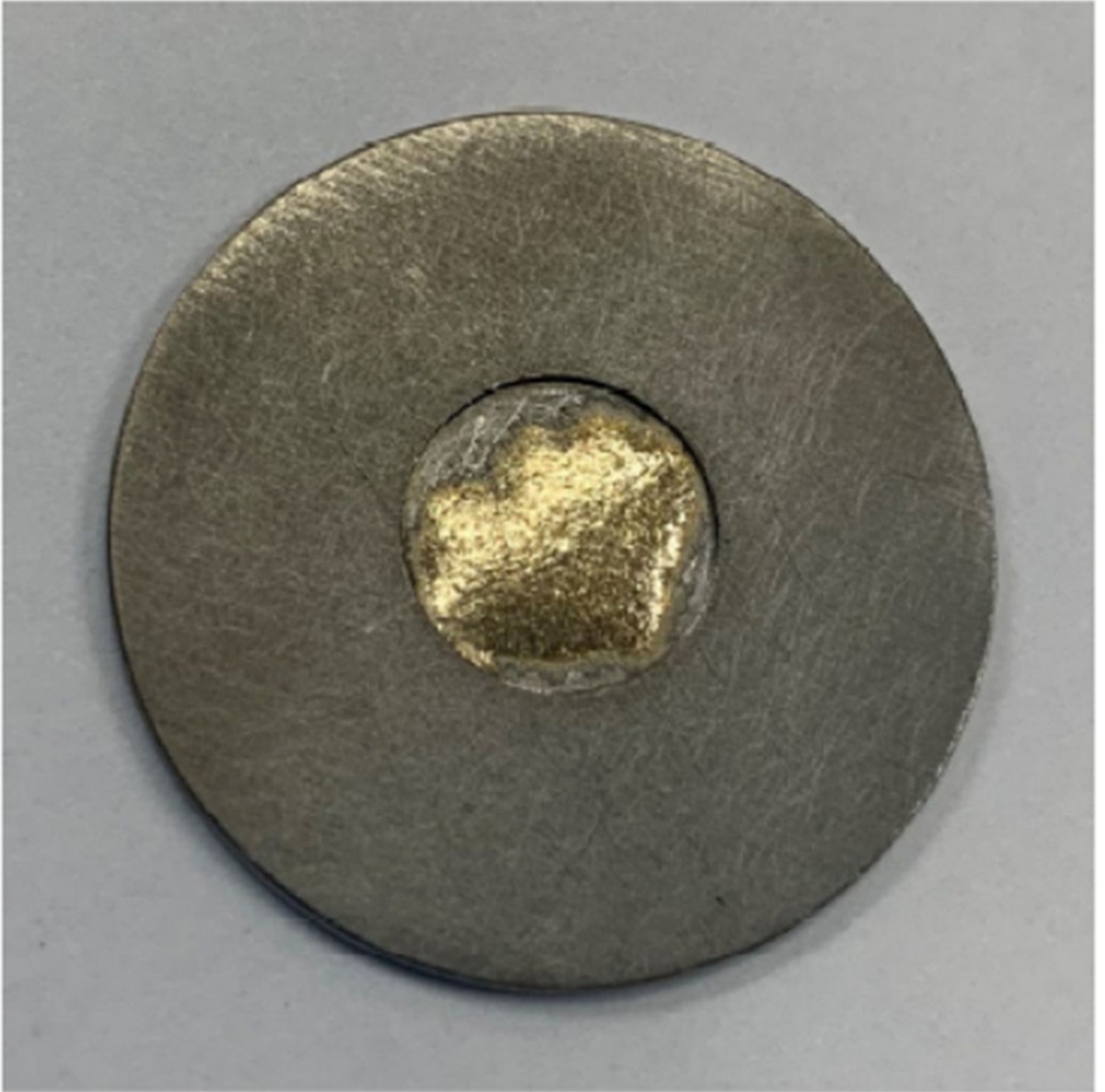
Fig. (7).
An example of gold targets sintered onto the tantalum backing before irradiation. (*A higher resolution / colour version of this figure is available in the electronic copy of the article*).
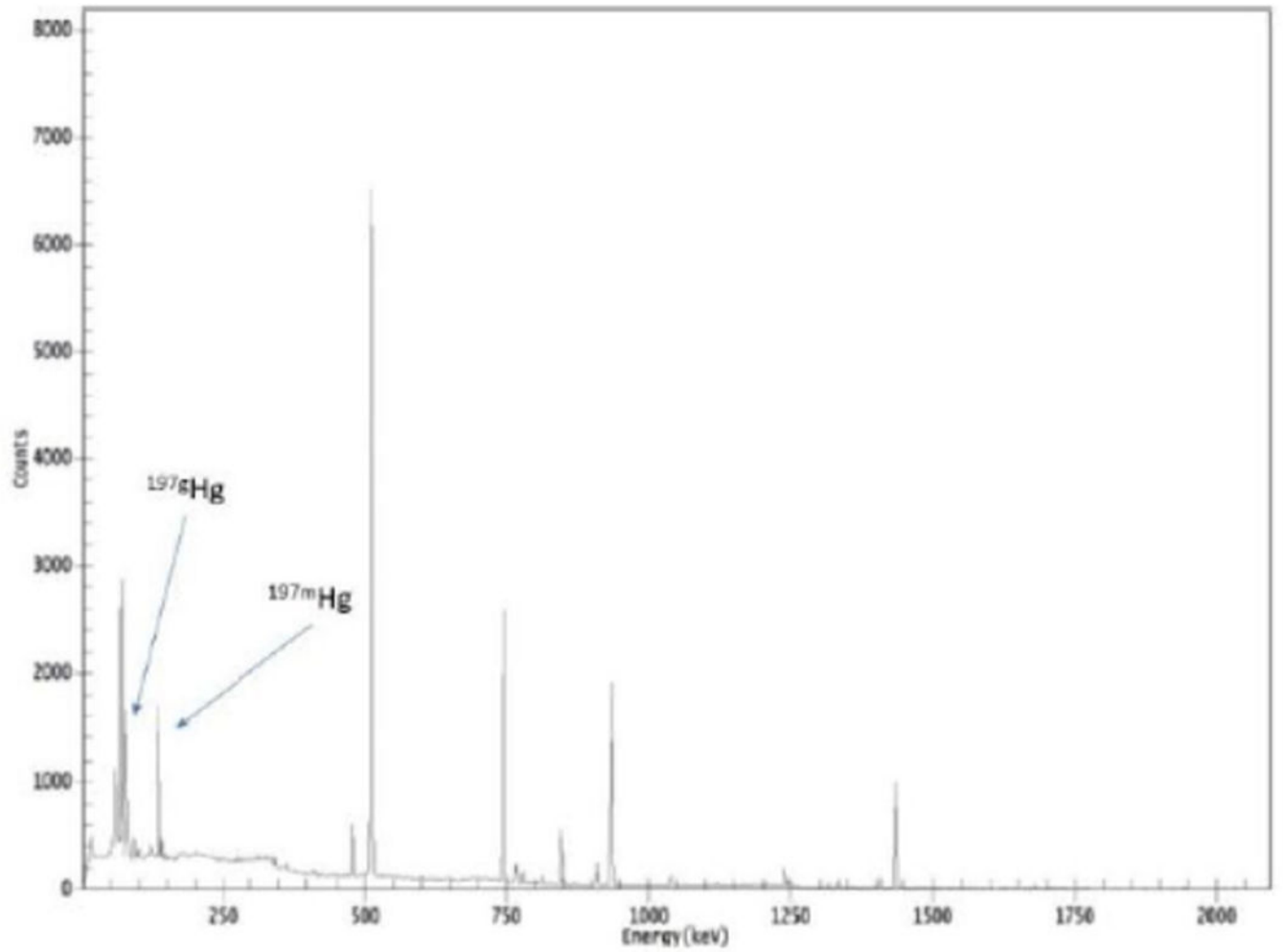
Fig. (8).
Example of a gamma spectrum of irradiated AuNP solution for 5 min at 20 μA. ^{197g}Hg was identified based on the 77.35 keV gamma line (18.70% branching ratio) and 197mHg was identified based on the 133.99 keV gamma line (33.50% branching ratio).
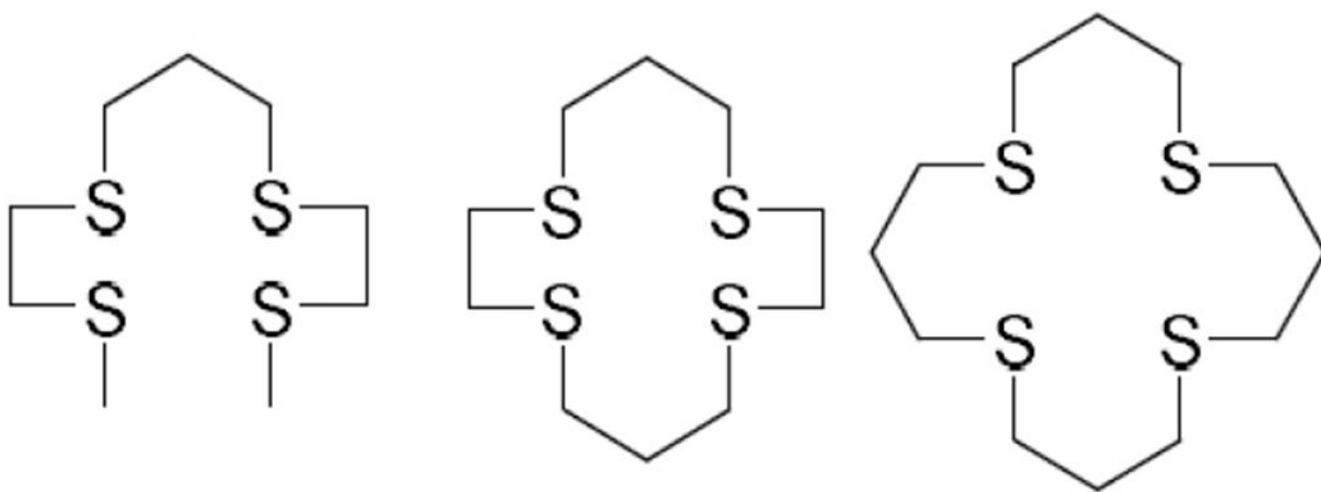
Fig. (9).
Cyclic and acyclic sulfur-rich ligands used to determine the effects of the macrocyclic effect within complexes [148,149].
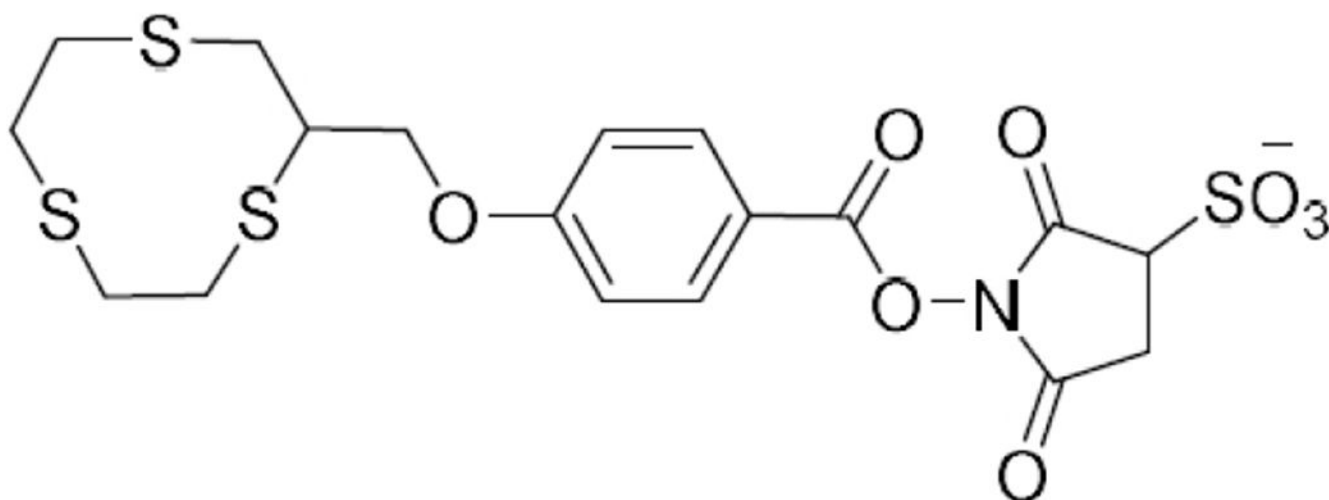
Fig. (10).
The trithiamacrocycle covalently conjugated to a linker for antibody attachment [150].
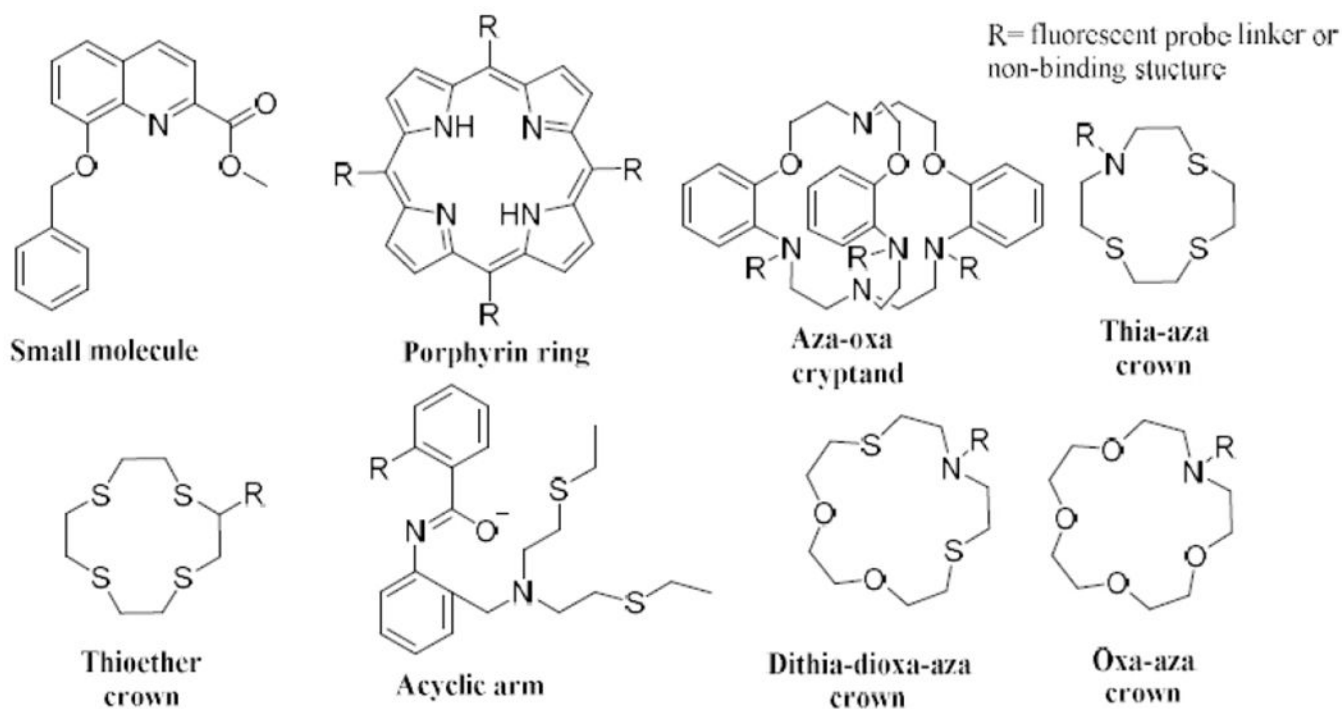
Fig. (11).
Examples of the derivatives of dithia-dioxa-aza macrocycles, thioether crowns, thia-aza crowns, oxa-aza crowns, porphyrin rings, calixarene, aza-oxa cryptands and acyclic arms or small molecules which have been incorporated into mercury sensing fluorescent probes [165,167,168,171–177].
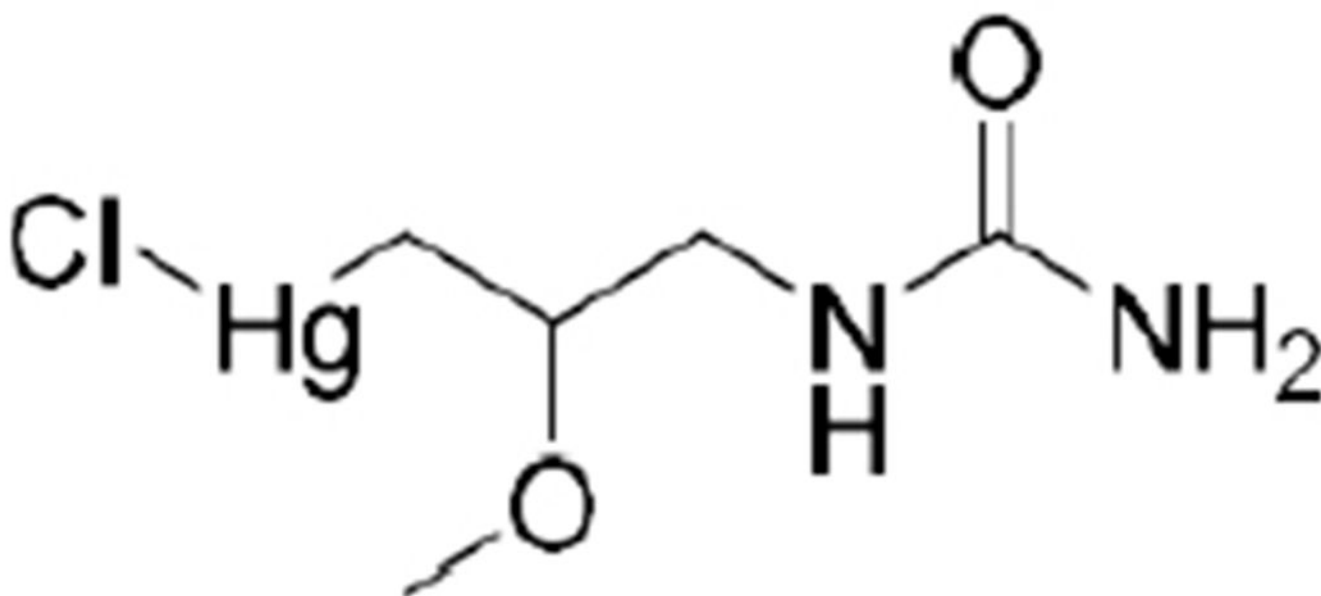
Fig. (12).
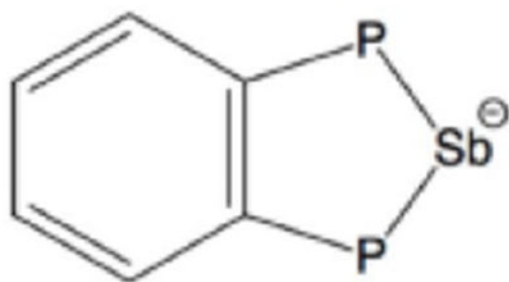Structure of chlormerodrin (3-chloromercury-2-methoxyprop-1-yl), an imaging agent using $^{197m/g}$Hg in the 1960s.
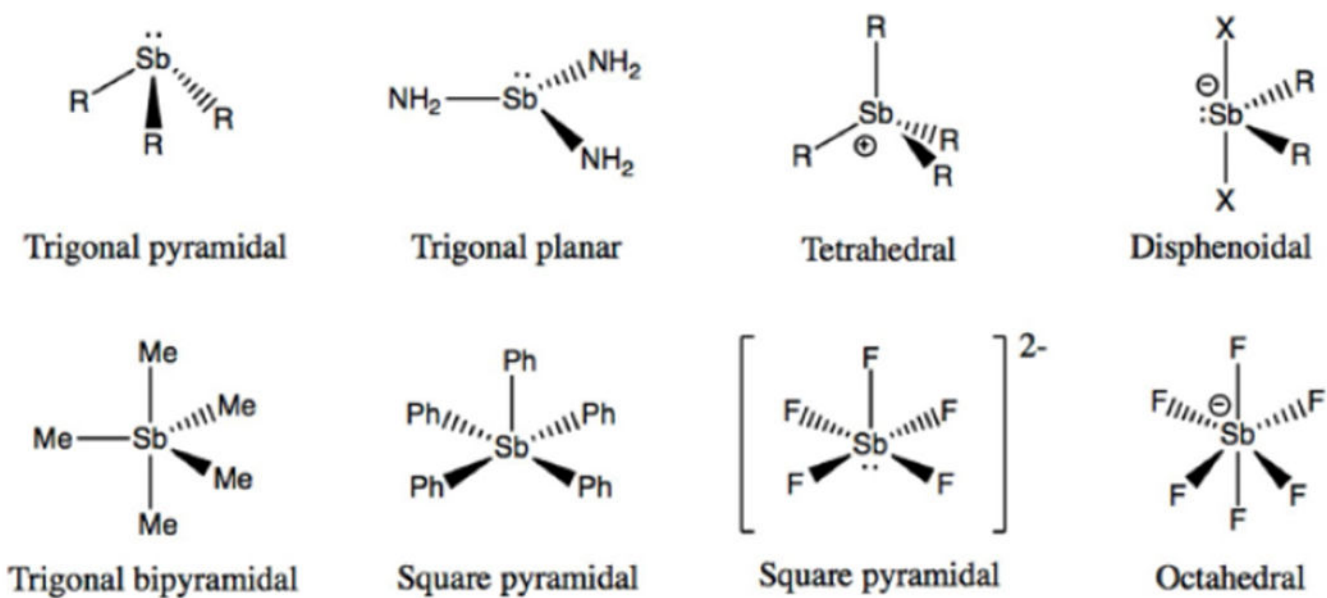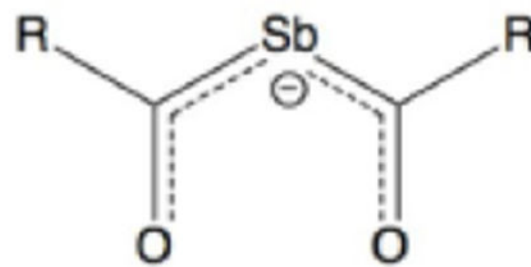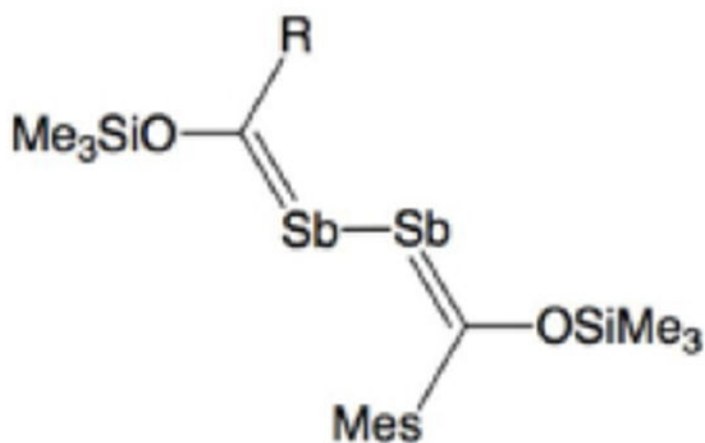
Fig. (13).
Example geometries commonly encountered in Sb coordination numbers and modes.
Adapted from [187].

diphospha-substituted antimonide
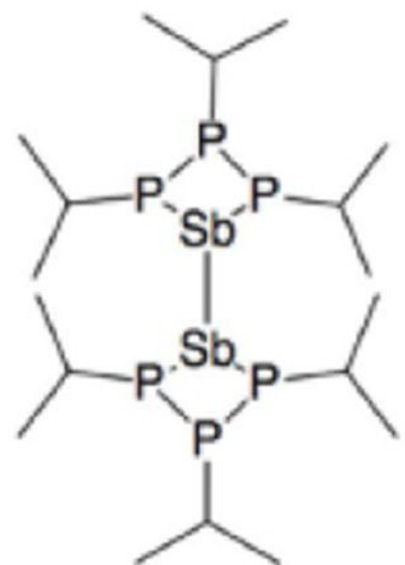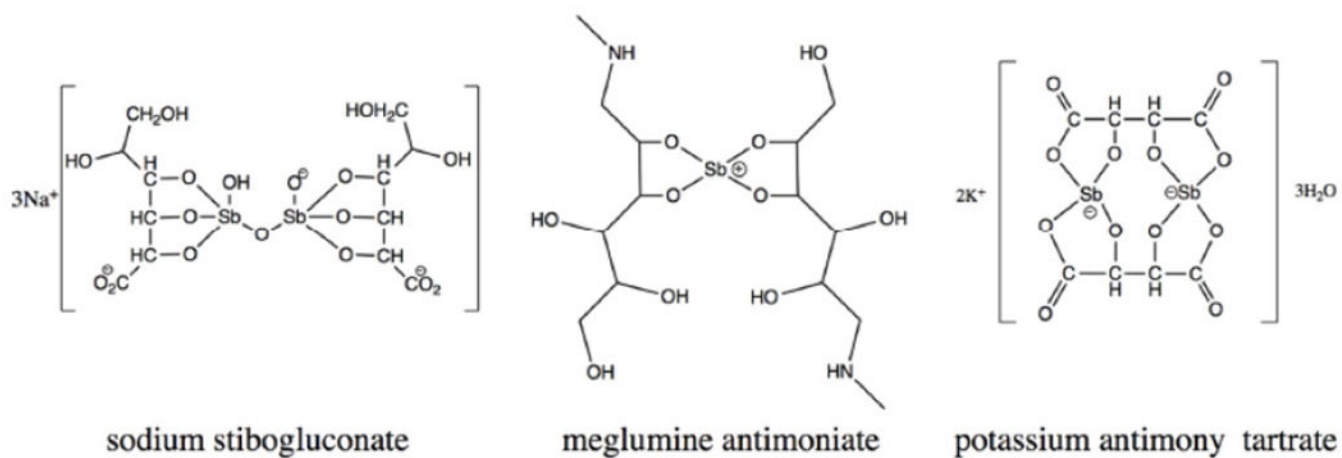
2-stiba-1,3-dionato

2,3-distibabutadiene

$[(Bu^tP)_3Sb\text{-}Sb(PBu^t)_3]_2$

Fig. (14).
Stibine containing organometallic structures [191].

Fig. (15).
Stibonate compounds used historically in medicine, though precise structures uncertain proposed structures have been reported [195].

Table 1.

The most promising radionuclides for MAE therapy with their characteristics. The MAE yield is the mean number of Meitner-Auger and Coster-Kronig electrons emitted per decay. The MAE energy is the average total energy of Meitner-Auger and Coster-Kronig electrons emitted per decay.

Radionuclide	Half-life	MAE Yield	MAE Energy (keV)	Refs.
[67]Ga	3.26 d	4.7	6.264	[15], [208]
[99m]Tc	6.01 h	4.0	0.889	[15], [208]
[111]In	2.8 d	14.7	6.75	[15], [208]
[123]I	13.2 h	14.9	7.419	[15], [208]
[125]I	60.1 days	24.9	12.241	[15], [208]
[197m]Hg	23.8 h	19.4	7.6	[39]
[197]Hg	2.67 d	23.2	7.4	[39]
[119]Sb	1.59 d	23.68	8.86	[39, 79]

Table 2.

Mean absorbed dose per unit cumulated activity (Gy Bq^{-1}) distributed in different human organs (ovaries, testes and the liver) from the MAEs and other radiations of ^{197m}Hg and ^{197g}Hg [20].

Radionuclide	Ovaries		Testes		Liver	
	MAE	Other	MAE	Other	MAE	Other
^{197m}Hg	1.9×10^{-13}	3.01×10^{-12}	5.99×10^{-14}	9.56×10^{-13}	1.17×10^{-15}	1.99×10^{-14}
^{197g}Hg	2.17×10^{-13}	8.23×10^{-13}	6.82×10^{-14}	2.66×10^{-13}	1.3×10^{-15}	6.29×10^{-15}

Table 3.

Comparison of single-strand break (SSB) and double-strand break (DSB) yields in per gigabase pair (GBp) per decay simulated within [56].

-	^{125}I	^{119}Sb	^{123}I	^{111}In	^{99m}Tc
Total SSB (Gbp^{-1} decay^{-1})	4.6	3.6	2.5	2.3	1.4
Total DSB (Gbp^{-1} decay^{-1})	0.38	0.31	0.21	0.20	0.013

Table 4.

Comparison of S-value calculations units Gy/Bqs reported within literature.

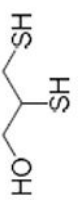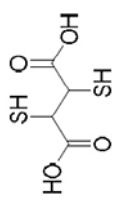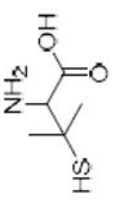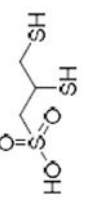| r_c	r_N	S(N ← N) [55]	S(N ← N) [56]	S(N ← N) [57]
5	2	0.0372	0.0309	0.0394
5	3	0.0128	0.00953	0.0142
5	4	0.00616	0.00418	0.00716
8	6	0.00234	0.00132	0.00272
9	7	0.00162	0.000853	0.00186
10	9	0.000874	0.000415	0.00097

Table 5.

Summary of literature-reported ^{119}Sb production methods and radionuclidic impurities. Side reactions exclude reactions with energy thresholds below that of desired reaction and half-lives < 1 h.

-	Incident Particle	Nuclear Reaction	Q (MeV)	Side Reactions / Residual $t_{1/2}$	Refs.
Direct	p	^{119}Sn(p,n)^{119}Sb	−1.37		[79, 209–211]
	p	^{120}Sn(p,2n)^{119}Sb	−10.48	^{120}Sn(p,n)^{120m}Sb / 5.76 d	
	d	^{118}Sn(d,n)^{119}Sb	2.89		
	d	^{119}Sn(d,2n)^{119}Sb	−3.60	^{119}Sn(d,n)^{120m}Sb / 5.76 d	[212, 213]
Indirect	p	^{121}Sb(p,3n)^{119}Te	−19.34	^{121}Sb(p,n)^{121m,g}Te / 164.2 d, 19.17 d ^{121}Sb(p,pn)^{120m}Sb / 5.76 d	[86, 111, 112, 214-216]
	p	^{123}Sb(p,5n)^{119}Te	−35.11	^{123}Sb(p,3n)^{121m,g}Te / 164.2 d, 19.17 d ^{123}Sb(p,n)^{123m}Te / 119.2 d ^{123}Sb(p,pn)^{122}Sb / 2.72 d	-
	p	^{nat}Sb(p,x)^{119}Te		^{121}Sb(p,5n)^{117}Te / 62 m à ^{117}Sb, 2.8 h ^{121}Sb(p,4n)^{118}Te / 6.00 d à ^{118m}Sb, 5.00 h ^{121}Sb(p,n)^{121m,g}Te / 164.2 d, 19.17 d ^{123}Sb(p,3n)^{121m,g}Te / 164.2 d, 19.17 d ^{123}Sb(p,n)^{123}Te / 119.2 d ^{121}Sb(p,pn)^{120m}Sb / 5.76 d ^{123}Sb(p,pn)^{122}Sb / 2.72 d	-
	d	^{121}Sb(d,4n)^{119}Te	−21.57	^{121}Sb(d,2n)^{121m,g}Te / 164.2 d, 19.17 d	[217]
	d	^{123}Sb(d,x)^{119}Te		^{123}Sb(d,4n)^{121m,g}Te / 164.2 d, 19.17 d ^{123}Sb(d,2n)^{123}Te / 119.2 d	-
	a*	^{116}Sn(a,n)^{119}Te	−9.99		[216, 218-220]
	a*	^{117}Sn(a,2n)^{119}Te	−16.93		[218]
		^{nat}Sn(a,x)^{119}Te		see footnote6	[221]

Alpha-induced reactions involving knockout of more than two neutrons are not included because of the unavoidable creation of 121 m,gTe, and the number of reactions initiated by irradiation of ^{nat}Sn, which has 10 stable isotopes, is so large as to make this material impractical for production of radioisotopically pure ^{119}Sb.

Table 6.

The structure and Hg^{2+} complex stability constants (of a 1:1 ML complex) of the current ligands used for Hg poisoning.

Structure	Name	Acronym	logβ	Refs.
	2,3-Dimercaptopropanol	BAL	48.8±0.1 [*]	[173, 174, 176, 178]
	2,3-Dimercaptosuccinic acid	DMSA	28.5±0.1 [*]	[176, 177]
	D-penicillamine	DPEN	37.8-38.3±0.1 [*]	[174-176, 178]
	2,3-Dimercapto-1-propanesulfonic acid	DMPS	42.2±0.1 [*]	[174-176, 178]

[*] logβ determined by potentiometric titrations.